Impact of charged silica nanoparticles on the biophysical properties of lung surfactant

Abdullah Khan

A Thesis
in
The Department
of
Chemistry and Biochemistry

Presented in Partial Fulfillment of the Requirements
for the Degree of Master Science (Chemistry) at
Concordia University
Montréal, Québec, Canada

May 2018

CONCORDIA UNIVERSITY

School of Graduate Studies

This is to certify that the thesis prepared

By:

Entitled:

and submitted in partial fulfillment of the requirements for the degree of

Master of Science (Chemistry)

complies with the regulations of the University and meets the accepted standards with respect to originality and quality.

Signed by the final examining committee:

Dr. Yves Gélinas Chair

Dr. Louis Cuccia Examiner

Dr. Peter Pawelek Examiner

Dr. Christine DeWolf Supervisor

Dr. Antonella Badia Co-Supervisor

Approved by

Chair of Department or Graduate Program Director

_____ 20____

Dean of Faculty

ABSTRACT

Impact of charged silica nanoparticles on the biophysical properties of lung surfactant

Abdullah Khan

As oxygen is inhaled it has to first cross a very thin layered membrane, lung surfactant, before it can enter the bloodstream. This lung surfactant membrane is composed of saturated and unsaturated phospholipids and membrane proteins which serve to reduce the surface tension at the air-liquid interface of the alveoli preventing alveolar collapse. To maintain this function through repetitive compression-expansion cycles, the film employs a mechanism of reversible reservoir formation and exhibits a high degree of fluidity. The inhalation of nanoparticulate may interfere with the functional properties of pulmonary surfactant including lowering the film collapse, altering viscoelastic properties and modifying lipid reservoir formation. This study aims to determine the degree to which nanoparticles interfere with the phase structure, compressibility, and viscoelastic properties when they deposit on the lipid membrane. The lung surfactant films are modelled using monolayers comprising either lipid-only mixtures or a natural membrane extract, namely Infasurf (a clinical formulation containing both extracted lipids and proteins). Surface pressure-area isotherms, Brewster angle microscopy, rheological measurements and grazing incidence x-ray diffraction data of films in the absence and presence of cationic and anionic silica nanoparticles are presented and discussed. The charge was found to play an important role with cationic nanoparticles having a greater impact on structural properties while anionic nanoparticles affect the viscoelastic properties of the films.

ACKNOWLEDGEMENTS

First and foremost I would like to thank God Almighty for all His blessings.

Secondly, I would like to thank both of my supervisors, Dr. Badia and Dr. DeWolf, for all their guidance and help throughout my M.Sc. degree, Dr. Behyan for teaching and guiding me with the diffraction data analysis and Dr. Schmidt for his help with instrumentation but also for his help in and out of the lab.

Additionally, I would like to thank all my labmates who have made this such an amazing experience.

Last but certainly not least, I would like to thank my wonderful parents and siblings, and my Precious for continuously supporting and encouraging me throughout this process.

This would not have been possible without all of you.

Abdullah

Table of Contents

List of figures

List of tables

List of abbreviations

APS:	advanced photon source
BAM:	Brewster angle microscopy
C:	condensed
DLPC:	1,2-dilauroyl-sn-glycero-3-phosphocholine
DLS:	dynamic light scattering
DOPC:	1,2-dioleoyl-sn-glycero-3-phosphocholine
DPPC:	1,2-dipalmitoyl-sn-glycero-3-phosphocholine
DPPE:	1,2-dipalmitoyl-sn-glycero-3-phosphoethanolamine
DPPG:	1,2-dipalmitoyl-sn-glycero-3-phosphoglycerol
ETS:	environmental tobacco smoke
FDA:	food and drug administration
FWHM:	full width at half maximum
GIXD:	grazing incidence x-ray diffraction
GRAS:	generally recognized as safe
LC:	liquid-condensed
LE:	liquid-expanded
LS:	lung surfactant
LSRT:	lung surfactant replacement therapy
NN:	nearest neighbour

NNN:	next nearest neighbour
NP:	nanoparticle
NRDS:	neonatal respiratory distress syndrome
PAT:	profile analysis tensiometer
PC:	phosphatidylcholine
PG:	phosphatidylglycerol
POPC:	1-palmitoyl-2-oleoyl-sn-glycero-3-phosphocholine
POPG:	1-palmitoyl-2-oleoyl-phosphatidylglycerol
SP-A:	surfactant protein A
SP-B:	surfactant protein B
SP-C:	surfactant protein C
SP-D:	surfactant protein D
STR:	step through rheology
THD:	total harmonic distortion
T_m:	transition temperature

Chapter 1. Introduction and literature review

During the industrial revolution a significant advancement in technology was observed and with time technology has had an exponential growth. However, the growth in technology did come at a price; a steady rise in the use of coal, oil and gas was also seen. The use of such fossil fuels have caused an increase in the amount of airborne pollutants. The negative impacts of these pollutants are not solely observed on the environment but on humans and other living creatures as well. Acid rain, ozone layer depletion and global climate change are a few of the environmental effects of such pollution. Examples of health impacts of airborne pollution include irritation of eyes and throat, coughing and breathing difficulties and more increased chances of developing/worsening lung and heart problems. The focus of the thesis is on the impact of pollution on respiratory processes. A short review of some of the common respiratory irritants (ozone, tobacco smoke and particulate matter) and their impact upon inhalation on the respiratory system will be presented.

1.1. Ozone

Ozone, a powerful oxidizing agent, is mainly found in stratosphere but its presence in the troposphere is a result of reactions taking place with other atmospheric pollutants which lead to the formation of tropospheric ozone. Since the beginning of the industrial era ozone levels have been on the rise causing an increase from 10 ppb (in 19th century) to 45 ppb (until mid-20th century). This rise can be attributed to the increased use of fossil fuel and other sources of NO_2 emissions[1]. The increase in ozone concentrations does not only affect the climate but also negatively impacts human health, more specifically the respiratory system. Basha *et al*. showed inflammation in the airways of asthmatic males when exposed to 200 ppb ozone concentration, this inflammation was not observed in non-asthmatic males undergoing the same exposure time and condition, although the exposure did not cause a decrease in lung function capabilities[2]. On the other hand other studies have shown that ozone exposure does lead to a decrease in lung function, however, these studies were not conducted by direct ozone exposure in controlled environment but rather dependent on environmental exposure. More recent *in vitro* research with model lung surfactant membranes have shown that exposure to low levels of ozone cause dendritic cell retention in lung tissue, partial unfolding of surface active protein SP-B and

resulting in loss of function and causes rearrangement of lipids at the air-water interface[3,4,5]. All of these effects impair proper lung surfactant functioning.

1.2. Environmental tobacco smoke

Environmental tobacco smoke (ETS) is another source of airborne pollutant with negative impacts on the respiratory system. There are over 4000 compounds in tobacco of which 60 compounds are known carcinogens such as benzene, nickel, aromatic hydrocarbons, nitrogen dioxide, sulphur dioxide, etc. ETS also contains particulate matter, including nanoparticles ranging between 10 nm to 700 nm with the majority being around 150 nm, a size range of particulate that can travel deep into the lung[6,7]. Larsson *et al*. have shown that exposure to ETS, a major source of lower airway irritant, during childhood increases the chances of being diagnosed with asthma later on in life, even in cases where the patient is a non-smoker[8]. Other studies reveal that daily exposure to ETS, residential or in the workplace environment, has been linked with increased chances of lung cancer in adults (smokers and non-smokers)[9]. More specifically, exposure to ETS causes lung surfactant to rigidify, alters the monolayers ability to re-spread, and removal of unsaturated lipids from the air-water interface. Such changes are prone to cause inflammation and impairment of the lung surfactant[10,11].

1.3. Environmental pollutants (fine particulate matter)

Nanoparticle research for use in various fields may be relatively new, however, nanoparticles have always been present. Recent technological advances have enabled their visualization and characterization. Nanoparticles are generated on a daily basis from natural and man-made sources; studies show that 90% of the suspended particulate matter in the atmosphere (aerosol) come from natural sources whereas the remaining 10% come from man-made sources[12].

Dust storms occurring in the Salton Sea, Sahara Desert and the Namibian desert lands, amongst seven other major regions, have been shown to be the major source, almost 50%, of natural nanoparticles that are present in the atmosphere. Not only do these particles have varying size range (nanometer to micrometer), but they also have very long migration times, therefore, even though the storm may be taking place in the Indus Valley, the nanoparticles can travel to regions that are much further away[12-14].

Forest fires also result in an increase in nanoparticle concentration in the air which can then travel and affect people that are located far away from the fire[15]. Lastly, although their occurrence is not very frequent, volcanic eruptions release a significant amount of gas, ash and particulate matter in the nanometer to micron range into the atmosphere which affects the environment around the volcanic region[12].

Nanoparticles generated from these natural sources can cause minor health impacts such irritation of the nose, throat, eye and skin and worsen respiratory conditions for patients that are diagnosed with asthma and emphysema but it can also lead to more serious diseases such podoconiosis, Kaposi's sarcoma, scarring of lung tissue and can even lead to death in some cases[12,16-18].

In addition to naturally generated nanoparticles, anthropogenic nanoparticles are also being generated on a daily basis due to the use of cars, trains and other sources of transportation that use fossil fuel and it is the main source of man-made nanoparticles in the atmosphere[19]. The nanoparticles generated by such engines vary between 20-130 nm[20]. Nanoparticles are also released into the atmosphere in construction and demolition sites. When driving by such sites, thick clouds can be observed that are covering the area and the workers are asked to wear proper gear to protect themselves. Studies done have shown that toxic particles varying between nanometer to micrometer range of lead, glass, asbestos fibers, tar and others can be found at such sites and it can also travel with the air to affect the surrounding areas[21].

It is not only the outdoor air that gets polluted on a daily basis, the air indoors can also be polluted with nanoparticles. For example, in some regions cooking is done by burning wood in a room that often does not have proper ventilation. In regions where electricity is not very common candles are used for light. Even vacuum cleaners release nanoparticles in the air. Other sources of nanoparticles that can be found inside the house are dead skin cells, particles from our clothes and for those who smoke indoors there is a plethora of carcinogenic nanoparticles present in such households[22-24]. These man-made nanoparticles also have negative health impacts: even though nanoparticle from dead skin cells, vacuum cleaners and clothes are not deadly they can irritate the lower airway tract and cause an asthma attack for those diagnosed with the disease. Nanoparticles from burning wood, exhaust fumes, construction and demolition sites, candles and

cigarette smoke, however, have more serious consequences. They can lead to increased chances of developing nasal, lung and pancreatic cancer, cardiovascular diseases, genetic mutations, lower respiratory tract illnesses such as pneumonia and bronchitis, asthma and death in children under the age of 5 due to smoke inhalation[25-29].

1.4. Engineered nanoparticles

The advancement in technology has not only allowed the creation of devices that are more efficient than their older counterparts but are significantly smaller in size as well. Although nanotechnology has its advantages, it has also introduced a new problem that may be affecting people who are involved in the production line. The use of nanoparticles has become widespread due to the number of applications that are now trying to incorporate these nanoparticles in their products. Some examples of their uses are as follows: they are used for cancer therapy and drug delivery in the biomedical and health industry, used for water resistant coatings and other types of food packaging in the food and agriculture industry, used for making ferro fluids, quantum computers and high density data storage devices in the electronics industry and for making anti-stain, medical, heat retaining textiles in the textile industry amongst numerous other uses. These nanoparticles are being incorporated into a wide variety of products for personal use but there is still limited understanding of the fate and impact of such nanoparticles on cells and biological systems.

The large number of applications dictates the necessity for a large variety of nanoparticles. The particle core can be changed to serve different purposes. One of the most common nanoparticle cores is gold which is proposed for many applications, such as a sensor to detect for arsenic in water samples[30]. Silica nanoparticles have been used for cancer therapy, in which they were used as drug carriers that release drugs in a controlled fashion[31], these particles have also been used for making more durable and anti-aging computer cables[32]. Two other very common nanoparticles that are used in the food, medical and cosmetics industry are zinc oxide and titanium dioxide nanoparticles; these particles are present in toothpaste, cosmetics, sunscreen lotions, paint, vitamin supplements, outer shell for medicines and in food as food coloring and food additives for various purposes[33,34]. There are many other nanoparticles that are used that have different particle core.

Another variable that can be manipulated is the particle coating, which is frequently used to give them specific functionality. For example, when nanoparticles are used as drug carriers and the coating confers biocompatibility, specificity for certain targets and/or protection from the environment and prevention of early drug release.

Nanoparticles also come in very different shapes and sizes, moreover, they can either be solid or hollow on the inside based on their use. Lastly, nanoparticles can have different charges on their surface, they can be cationic, anionic or neutral. This gives an insight in the vast number of different nanoparticles that are present and the variability of their properties. Nanoparticles used for paint, food, cosmetics, toothpaste and medicine are synthesized in bulk quantities and not only the workers present in manufacturing facilities but the general public that use such products are also exposed to these nanoparticles.

Although these nanoparticles have been approved by the FDA as GRAS (Generally Recognized As Safe) studies have shown that these nanoparticles are not as harmless as initially predicted[33]. The extent of health effects are not known for all of the different types of nanoparticles that are present but numerous studies have been done to show the negative health impacts that some of these nanoparticles are causing.

Beryllium nanoparticles which are used for making electronic parts and plastic molds have been known to cause allergic reactions, pneumonia, heart enlargement and higher chances of lung cancer[35,36]. Cadmium nanoparticles which are used for making batteries, plastics and metal coatings have been shown to cause and linked with nausea, emphysema, liver damage and cancer of the lungs, stomach and pancreas[37,38]. Aluminum nanoparticles which are present in antacids, antiperspirants, deodorants, food and other commercial products have been linked with bone disease, breast cancer and dementia, although debate is still ongoing whether or not Alzheimer's disease is directly caused by excess exposure to aluminum nanoparticles[39-42]. Miners and welders have an increased exposure to manganese nanoparticles, which have been showed to cause neurological diseases, most commonly Parkinson's disease[43,44]. Silica nanoparticles which are present in numerous consumer products such as paint, rubber and plastics have been shown to cause scleroderma, rheumatoid arthritis and lung cancer, although the association of silica nanoparticle exposure and lung cancer is still heavily debated[45,46]. Although not all of these

diseases are caused by nanoparticles, studies have shown that nanoparticle exposure seems to aggravate the conditions of patients that have been diagnosed with some of these diseases. For this research, the focus will be the effect of nanoparticle inhalation as a first route of entry which affects the lungs.

1.5. Lung surfactant composition and function

In humans, respiration takes place in the lungs. As we inhale, oxygen is brought inside the lungs and as we exhale, carbon dioxide is expelled out. The exchange of oxygen and carbon dioxide occurs inside the alveoli found inside the lungs. When oxygen is brought inside the body, it has to first cross a very thin layered membrane film called the lung surfactant before it can enter the bloodstream. Lung surfactant (LS) is a lipid protein monolayer film that coats the inner surface of the alveolar sacs and its role is to reduce the surface tension of the alveolar sacs to prevent alveolar collapse during the breathing cycle[47,48]. LS is composed of 80-90% phospholipids (of which 70-80% consists of saturated lipids and 20-30% unsaturated lipids), 5-10% surfactant associated proteins (which consists of SP-A, SP-B, SP-C and SP-D where SP-B and SP-C are surface active proteins and SP-A and SP-D are non-surface active proteins) and 3-10% neutral lipids (which mainly consists of cholesterol)[49-55]. Of the 70-80% saturated PC lipids that are present in lung surfactant, 1,2-dipalmitoyl-sn-glycero-3-phosphocholine (DPPC) is the major PC lipid and of the 20-30% unsaturated PG lipid, 1-palmitoyl-2-oleoyl-phosphatidylglycerol (POPG) is the major PG lipid[56]. Each of these components play a specific role for proper lung surfactant function. Figure 1 shows a schematic of the inner surface of the alveolar sac depicting the breathing process. During inhalation LS is at its most expanded state (Step 1), the lipids and proteins are present but they are not in a highly compressed state. As exhalation starts, the film is compressed which brings the lipids and proteins closer together and there is a phase separation that occurs between the saturated and unsaturated lipids (Step 2). With further compression the unsaturated lipids that are not stable at high surface pressures (low surface tensions) are expelled from the air-water interface (Step 3). The expelled lipids are held in lipid reservoirs anchored by the SP-B and SP-C proteins, this process is termed the “squeeze out” (Step 4). The formation of these reservoirs allows for easy reincorporation of the collapsed material back into the monolayer during inhalation, prevents lipid loss during breathing cycle and allows the monolayer film to reach much higher surface pressures without collapsing.

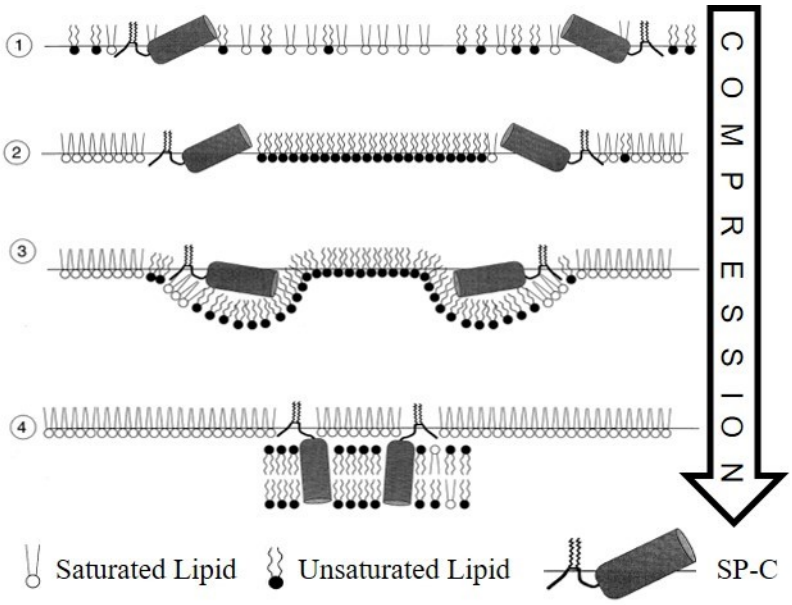

Figure 1. Schematic depicting lung surfactant activity from inhalation to exhalation[57]. Adapted from Veldhuizen *et al., Biochimica et Biophysica Acta,* 2000.

1.5.1. Roles of saturated and unsaturated phospholipids

Both saturated and unsaturated lipids play an important role for proper LS functioning. Saturated lipids allow LS to reach very low surface tensions during exhalation whereas unsaturated lipids allow LS to rapidly compress and expand during the breathing process[50]. Figure 2 is a schematic isotherm depicting the different phases a phospholipid can undergo during compression and will be used to better explain lung surfactant functioning. At higher molecular area the lipids are in the gaseous phase, in this phase the lipid tails have plenty of space and are not restricted in conformation. During the gaseous phase, surface pressure stays constant at 0 mN/m with decreasing molecular area. As the monolayer is further compressed (and the molecular area decreased) the surface pressure starts to increase. The molecular area at which the pressure begins to increase is called the critical area. This phase transition from the gaseous phase can result in the formation of a liquid-expanded (LE) or condensed (C) phase. In the LE phase the lipid tails are more restricted in mobility than they were in the gaseous phase but remain fluid with properties similar to a liquid alkane. If a subsequent LE-C transition is observed, this will be evidenced by a first-order phase transition plateau in which the pressure remains constant until all of the LE phase is converted to C phase. There are many different condensed phases,

including tilted and untilted phases. The phase diagrams for such films is well established. If there is a transition from a tilted (often called liquid-condensed (LC)) to an upright or untitled phase (often called solid-condensed), this transition is usually a second-order phase transition. At some point the film cannot be further compressed and remain monomolecular and the film buckles, a process known as collapse. DPPC undergoes all of the phase transitions shown in the schematic isotherm in Figure 2, except for the untilted phase, (chemical structure given in Figure 3). These lipids can achieve the high surface pressures (near-zero surface tensions) required to prevent alveolar collapse. On the other hand, the isotherm of an unsaturated phospholipid such as POPG (Figure 3) or a saturated phospholipid with short lipid tails will be significantly different. An unsaturated lipid, such as POPG, due to the presence of a unit of unsaturation which inhibits the lipid tails from adopting an all-trans, close-packed orientation required to form a condensed phase, will only stay in the LE phase until collapse (at room temperature). Additionally, the collapse will occur at a lower surface pressure compared to the collapse pressure of a saturated lipid. The fluid, LE phase of the unsaturated phospholipids maintains fluidity in the LS monolayer film and this fluidity allows the rapid compression and expansion of LS during the breathing cycle.

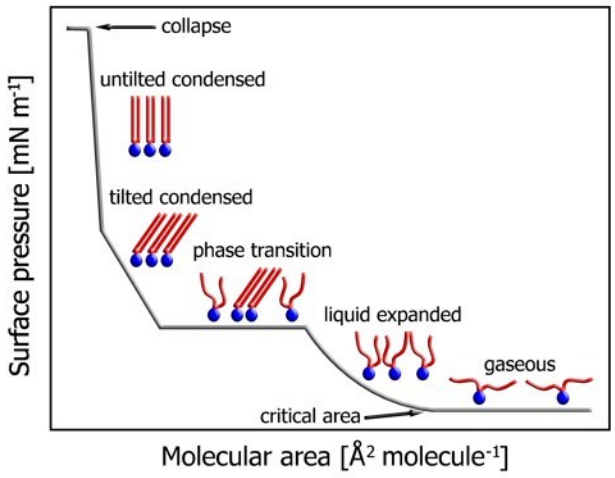

Figure 2. Schematic representation of a phospholipid isotherm with diagrammatic depictions of the various phases that can be observed.

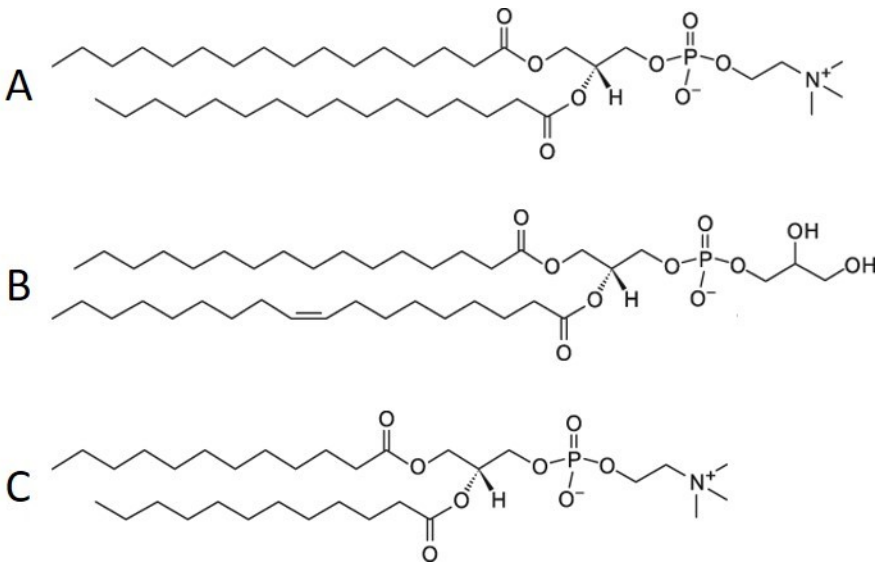

Figure 3. Chemical structure of (A) 1,2-dipalmitoyl-sn-glycero-3-phosphocholine (DPPC), (B) 1-palmitoyl-2-oleoyl-sn-glycero-3-phospho-1-glycerol (POPG) and (C) 1, 2-dilauroyl-sn-glycero-3-phosphocholine (DLPC).

1.5.2. Roles of lung surfactant proteins

There are four surfactant proteins associated with lung surfactant: SP-A, SP-B, SP-C and SP-D. SP-A and SP-D are not surface active while SP-B and SP-C reside within the lung surfactant film.

1.5.2.1. SP-A and SP-D

SP-A and SP-D are glycoproteins with molecular weight of 36 kDa and 43 kDa, respectively, that are produced by alveolar type II cells that belong to the collectin family, where members of this family are known to have host defense functions[58,59]. Earlier work to elucidate the roles of SP-A and SP-D had shown that they were involved in maintaining the surfactant lipid homeostasis and surface activity of LS. Two proteins, fibrinogen and albumin, cause severe inhibition of surface activity of LS lacking SP-A protein, however, once SP-A was added to LS, the inhibition caused by fibrinogen and albumin was completely reversed[60]. In the absence of SP-D protein enlargement of alveoli, accumulation of surfactant lipid and altered structural organization of phospholipids were observed in mice lung surfactant[59]. Both SP-A and SP-D have anti-inflammatory and pro-inflammatory roles; in naïve lungs these two proteins help minimise potential damage from continuous low level exposure from pathogens, allergens and

apoptosis. However, in the case of excessive exposure to pathogens, allergens and other foreign bodies these two proteins have pro-inflammatory roles to complement the innate and adaptive pulmonary immunity[61]. These two proteins, which can directly interact with the pathogen and stimulate immune cells, are also involved in protecting the lungs against invading bacteria and virus[58,62,63]. Although they have an important role to play in the proper functioning and protecting the lungs from pathogens, SP-A and SP-D are not surface active proteins and therefore are not taken into consideration for this project.

1.5.2.2. SP-B and SP-C

SP-B and SP-C are surface active proteins that are also produced by alveolar type II cells and are of interest for this research[57]. SP-B is an amphiphilic protein of 8.7 kDa, but in its functional form it is a homodimer weighing 17.4 kDa. At physiological conditions, it carries a net positive charge and therefore it can interact with the negatively charged POPG and other anionic lipids. Being amphiphilic, it also helps in membrane-membrane associations once monolayer squeeze-out takes place[52,56,57]. SP-B is also responsible for proper re-spreading of lipids during expansion of the monolayer. Ding *et al*. have shown that in the absence or at very low concentrations of SP-B, upon compression the monolayer will not fold into multilayer reservoirs rather the monolayer will crack when it collapses[52]. SP-C is a 4.2 kDa protein (the smallest of the lung surfactant proteins by weight) that is highly hydrophobic[57]. It resides within the monolayer and helps anchor the collapsed lipids during the breathing cycle by forming reservoirs below the air-water interface[64]. This protein also has palmitoyled chains, which helps in staying bound to the monolayer and it also helps in maintaining a liquid expanded phase throughout the breathing cycle[65]. Bringezu and Schurch have shown that SP-C is equally important for multilayer formation, lipid loss prevention and easy re-spreading of the lipids[10,66].

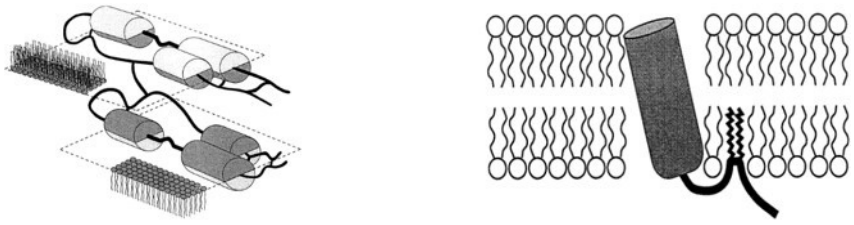

Figure 4. Schematic representation for SP-B and SP-C proteins[57].

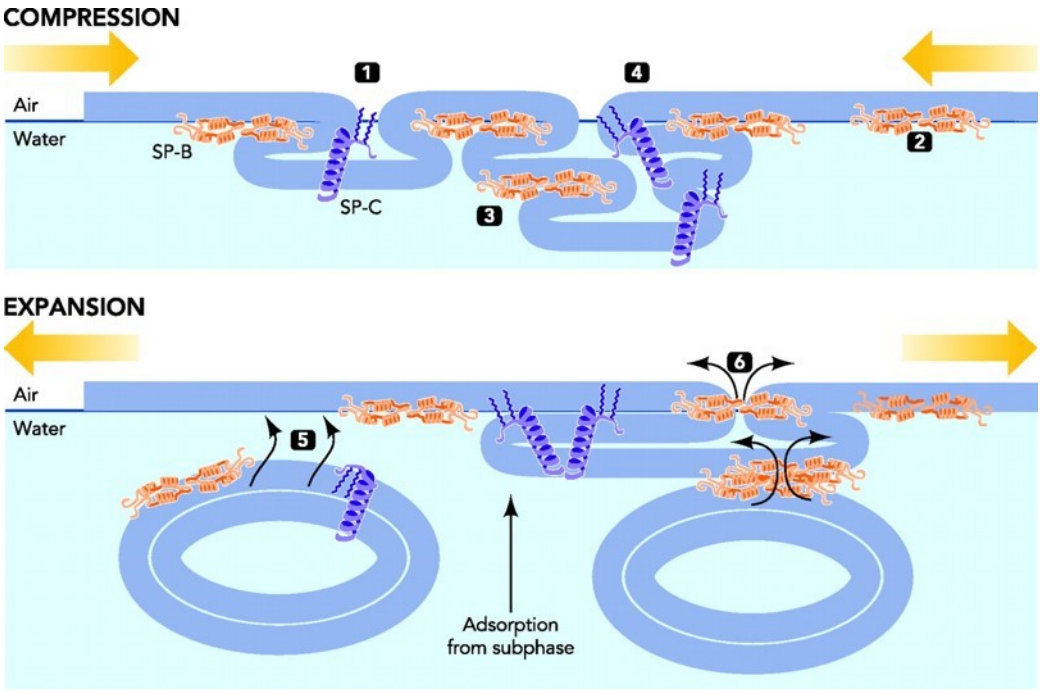

Figure 5. SP-B and SP-C during compression and expansion cycle[67].

1.6. Lung surfactant model membranes

Lung surfactant is a monolayer consisting of a complex lipid-protein mixture that is found on the inner surface of the alveoli. Although it is a complex mixture it has key components that allow for its proper function and using these key components simple model membranes can be made in-vitro to better understand LS functions. Langmuir monolayers are a very good mimic of LS films in-vitro since they are spread at the air-water interface and can be compressed-expanded as a LS film (i.e. using similar frequencies) inducing the required lipid phase separation. Using monolayers that have similar composition as LS enables the study of the structure and function of LS and in particular the roles of each LS component, testing of new drugs for neonatal respiratory distress syndrome (NRDS) and other possible respiratory diseases, and evaluation of the impact of airborne pollutants, such as tobacco smoke, ozone, fine particulate matter and nanoparticles, on proper LS function[27,33,48,56,58].

1.7. Model membrane systems

Many monolayer compositions have been used in literature to represent lung surfactant, from single component DPPC to more complex natural extracts comprising a lipid-protein mixture. Some of the most commonly used monolayer models are described below.

1.7.1. Lipid-only films

Of the key components identified from LS, phospholipids are one of the main components, consisting of 80-90% of LS, therefore they are used to make LS membrane mimics for *in vitro* experiments[50]. Studies have been done using single component systems, specifically DPPC or POPG, since they are the representative lipids for saturated and unsaturated phospholipids present in the LS. Studies have also been done using mixtures of lipids of DPPC, DPPE, DOPC, POPG, POPC, and other lipids to determine the effect of lipid chain length and headgroup charge on viscoelastic properties of the model lung surfactant films. Results show that monolayers formed with unsaturated lipids have lower elasticity, presence of unsaturation increases lipid disorder and the more hydrated the lipid headgroup is the deeper it will penetrate into the water subphase and as a result cause an increase in viscosity[52,68-70]. A ratio of 70:30 DPPC:POPG phospholipid model membrane is frequently used to represent lung surfactant[71-73].

1.7.2. Natural extracts of lung surfactant (lipid-protein mixtures)

Babies born before the 30 week term most often are associated with NRDS, which is a common problem in neonatal babies where the lungs are deficient in pulmonary surfactants, therefore, the lungs are not working properly and there is not enough gas exchange taking place[74]. The treatment for NRDS is lung surfactant replacement therapy (LSRT), where the babies are given supplemental lung surfactant to compensate for the deficiency. LSRT mainly consists of the necessary pulmonary surfactants which help with proper lung functions, where the non-surface active proteins (SP-A and SP-D) have been removed. There are numerous LSRTs available for use, such as Exosurf, Curosurf, Infasurf and Survanta to name a few, they are mainly derived from porcine or bovine lung lavages but they differ in lipid and protein concentrations[73].

Generic name	DPPC	DPPC:POPG(7:3)	Beractant	Poractant alfa	Calfactant
Trade name	–	–	SURVANTA®	CUROSURF®	INFASURF®
Source	Synthetic	Synthetic	Bovine lung mince	Porcine lung mince	Calf lung lavage
Phospholipids	100	100	84	99	91
PC/DPPC	100/100	70/70	71/50	69/47	79/43
PG	0	30	2.4	1.2	4.5
PE	0	0	3.4	4.5–7.4	2.8
PI + PS	0	0	1.3	4.5–8.4	4.0
LPC	0	0	1.5	1.0–7.0	< 1.0
SM	0	0	3.4	1.8–7.9	0.8
Neutral Lipids					
Cholesterol	0	0	< 0.2	0	5–8
Free fatty acids	0	0	5.8–14	n/a	0.64
Hydrophilic Proteins (SP-A)	0	0	0	0	0
Hydrophobic proteins	0	0	0.94	1.1	1.6–2.2
SP-B	0	0	0.04	0.4	0.9
SP-C	0	0	0.9	0.7	0.7–1.3

PC: phosphatidylcholine; DPPC: dipalmitoyl phosphatidylcholine; POPG: palmitoyl-oleoyl phosphatidylglycerol; PG: phosphatidylglycerol; PS: phosphatidylserine; PE: phosphatidylethanol; PI: phosphatidylinositol; LPC: lysophosphatidylcholine; SM: Sphingomyelin; SP: surfactant protein.

Figure 6. Lipid-protein compositions of the various lung surfactants that are used as model membranes[73]. This table is adapted from Zhang, H *et al*., *Biochimica et Biophysica Acta*, 2011, 1808, 1832-1842.

Of the many different LSRTs available Survanta, Curosurf and Infasurf are most commonly used to treat NRDS[75]. Curosurf is derived from porcine lung lavage and has phospholipids and the surface active proteins, however, the non-surface active proteins and cholesterol have been removed. Both Survanta and Infasurf are derived from bovine lung lavage, therefore, they should have very similar phospholipid composition and do not have surface-inactive proteins. They both have the surface active proteins (SP-B and SP-C) but in differing amount; Survanta is SP-C rich and has very small amount of SP-B protein whereas Infasurf is SP-B rich and has moderate amount of SP-C protein compared to Survanta and Curosurf, but the major difference between Survanta and Infasurf is that Survanta has added palmitic acid and DPPC[73].

Clinical studies done to compare the efficacy between Survanta and Infasurf have shown that whether for treatment or prevention of NRDS in neonatal infants the number of doses are the same between the two LSRTs. However, the interval time between doses are longer for Infasurf than it is for Survanta, in other words, Infasurf provides a longer lasting effect than Survanta[76]. Comparative studies between Survanta and Infasurf done by Notter *et al*. have shown that both Survanta and Infasurf had less total protein than natural LS, as proteins are lost during lung

lavage and extraction process, however, Survanta had a significantly lower protein content than Infasurf, more specifically Survanta was lacking SP-B protein. Primarily due to the lack of SP-B protein and other differences in lipid composition Survanta was unable to reach very high surface pressures relative to Infasurf[54]. In order to see whether the inability of Survanta to reach high surface pressures similar to Infasurf was due to the lack of SP-B protein, Notter *et al.* did comparison studies. The comparison was between Infasurf, Survanta and Survanta with additional SP-B protein. With the addition of SP-B protein Survanta showed similar values to that of Infasurf[54]. The importance of SP-B protein was also demonstrated by Ding *et al*. through the use of similar experiments of adding excess SP-B protein to a monolayer[52]. These LSRTs very closely resemble human LS and therefore using these as model membranes for research purposes can give very accurate results as to how human LS would be impacted in the presence of nanoparticles[77].

1.8. Lung surfactant model membranes and nanoparticles

A significant body of research has been undertaken to determine the impact of nanoparticles on the respiratory system. Both computational and experimental methods have been employed to study different model lung surfactant membranes with a variety of nanoparticle types (e.g. variations in size, shape, hydrophilicity and surface charge). An important parameter is whether the particles are co-spread (hydrophobic particles) with the lipid monolayer or added to the aqueous subphase (hydrophilic particles) beneath the lipid monolayer.

Lin *et al*. used computational methods to understand the effect of changing shape, size and hydrophilicity of the particles during the compression-expansion process. The simulated monolayer consisted of DPPC only, the nanoparticle sizes examined were 3 nm and 5 nm and the shapes tested were rod, barrel and disk. The nanoparticles were introduced from the air phase (placed on top of the monolayer) and both hydrophilic and hydrophobic nanoparticles were tested, the monolayer was then "spread" on top of the subphase. The hydrophilic nanoparticles were found to penetrate deeper into the monolayer to get closer to the hydrophilic headgroup whereas hydrophobic nanoparticles tend stay near the hydrophobic lipid chains. The larger the nanoparticle, the more lipids it pulls down into the subphase along with it during the compression and the more it affects the monolayer. In terms of shape, a rod shaped nanoparticle can penetrate the monolayer most easily compared to disc or barrel shaped nanoparticles

(rod>disc>barrel). The main reason behind this ranking is the contact area of the nanoparticle; rod shaped NPs have the smallest contact area, whereas barrel shaped NPs have the largest contact area and the disc shaped NPs have a contact area that is in between the two. The larger the contact area of the NP the more contact it will make with the monolayer and the harder it will be for it to penetrate below the monolayer[78].

There is a plethora of experimental work testing the impact of nanoparticles on lung surfactant model membranes. These studies focus on the hydrophobicity of the nanoparticles, surface charge and particle size. Moreover, nanoparticle concentration and method of introducing the nanoparticles into the monolayer is also tested. Focus is also placed on the type of monolayer being studied; there are simple monolayers which consist of one lipid (DPPC), a mixture of lipids (PG:PC lipids), lipid-protein mixtures and lipid-protein-cholesterol mixtures as well. Work done by Harischandra *et al.* has shown that hydrophobic polyorganosiloxane nanoparticles are attracted to the air-water interface and can form a nanoparticle monolayer[79]. Isotherms and compression-expansion cycles of DPPC:DPPG and DPPC monolayers in the presence of these hydrophobic polyorganosiloxane NPs (co-spread with the monolayer film) indicate that these NPs interact strongly with the lipid monolayer, disturb the domain structures formation by causing a fluidization of the monolayer and tend to be located around domain borders. Rheology studies carried out using a Langmuir trough with an oscillating barrier in the presence of hydrophobic NPs in DPPC monolayer have shown that NPs cause an increase in disorder of monolayer and hinders elasticity[80]. The rheological parameter viscosity is a measure of the fluidity or the ability of the film to spread and is dominated by lipid headgroup interactions with the subphase and neighboring headgroups whereas elasticity reflects the recovery of the film after the removal of stress which is dominated by lipid chain interactions[70].

Studies have also been done to observe the effects of 1 wt% of hydrophilic silica nanoparticles on model lung surfactant monolayers, where monolayers consisted of mixtures of DPPC, DOPC and cholesterol of differing amounts. Unlike the hydrophobic nanoparticles, that can form a nanoparticle monolayer at the air-water interface, the hydrophilic silica nanoparticles remain dispersed in the subphase and do not cause an increase in surface pressure upon compression of the barriers[81,82]. However in the presence of a monolayer these nanoparticles are attracted to the

surface and interact with the lipids present at the air-water interface. The interaction causes the isotherm to shift to higher molecular areas and the phase transition plateau to disappear[83].

The rheological properties of model membranes are indicative of their ability to rapidly compress and expand through the breathing cycle and have been used to evaluate the biological impact of inhaled particulate. In the presence of hydrophobic fumed silica nanoparticles for model lung surfactant membranes consisting of a single type of lipid Guzman *et al.* observed that the effect on rheology was that the oscillations were increasing in amplitude and thereby causing harmonic distortions, which indicates that there is nanoparticle incorporation with the monolayer film present at the air-water interface. Moreover, the presence of these hydrophobic fumed silica NPs caused an increase in disorder and hindered domain formation. The incorporation of these NPs to the lipid causes a strong steric hindrance and thereby prevents the normal function of the lipid monolayer[80].

Within the literature reports of nanoparticle impacts on lung surfactant films, the composition of the model lung surfactant membrane, the size, shape and type of nanoparticles and the methodology vary significantly. Despite this, a general consensus is emerging that nanoparticles causes distortions in domain formation, increases disorder in monolayer structure, causes fluidization of the monolayer and as a result proper functioning of the monolayer is affected.

1.9. Research objectives

Our research focuses on correlating the effect of nanoparticles on the structure, morphology and rheological parameters (viscosity and elasticity) of lung surfactant films. To understand the role of the model film and particle characteristics, both the lipid only and lipid-protein monolayers were studied as a function of membrane composition, particle concentration and particle charge. For this work three types of silica nanoparticles were chosen as they have widespread applications in construction materials and biomedical applications. Silica nanoparticles are surfactant free, low polydispersity, commercially available and have variable size, surface charge and particle coating. The nanoparticles used for this research were provided by AkzoNobel and include cationic, anionic and neutral silica nanoparticles that are of the same order of magnitude in size.

The four systems that were chosen for this work are DPPC, 70:30 DPPC:POPG mixture, 70:30 DPPC:DLPC mixture and Infasurf. The first three are lipid-only systems and the latter, Infasurf, is a natural extract comprising of lipids and proteins. DPPC is a saturated lipid found in high concentration in lung surfactant. It is frequently employed to represent the condensed phase of lung surfactant. Use of this single component system enables an understanding of one portion of the film but does not mimic the overall phase behaviour very well as it lacks a fluid phase at physiologically relevant surface pressures. A 70:30 DPPC:POPG mixture is used as a simple lung surfactant model without the proteins, chosen because both DPPC and POPG are found in high concentration in natural lung surfactant and a 70:30 ratio is a representative ratio of saturated and unsaturated lipids in lung surfactant[57,69,83]. This system forms a DDP-rich condensed phase and a POPG-rich liquid expanded phase. A 70:30 DPPC:DLPC mixture was chosen to keep the same ratio of condensed and liquid expanded phases but without the negative charge of POPG. DLPC, with the same zwitterionic headgroup as DPPC, has shorter lipid chains (C12) and so it stays in the liquid expanded phase until collapse. This system is used to evaluate the role of the charge of the fluid phase. Finally, Infasurf is a purified, natural lung surfactant extract and is used for lung surfactant replacement therapy. It is extracted from bovine and has the surface active SP-B and SP-C protein but not the SP-A and SP-D protein which are non-surface active.

The use of these systems will allow for a comparison between the effect of nanoparticles on lipid only versus lipid-protein monolayers and the effect of nanoparticles on differing amounts of protein in the system. Rheological changes were monitored using a profile analysis tensiometer (PAT) whereas surface activity was monitored using both a PAT and a Langmuir film balance. The Langmuir film balance was also coupled with Brewster angle microscopy to study the morphological changes taking place. Synchrotron Grazing Incidence X-ray Diffraction (GIXD) measurements are used to evaluate structural changes in the monolayers.

Of particular note, most studies focus on relatively high concentrations on nanoparticles. For hydrophilic nanoparticles dispersed in the subphase, these concentrations are often close to 1 wt%. In this work, the effect of 0.001% cationic, anionic and neutral silica nanoparticles on the different model lung surfactant membranes is studied; this concentration is the lowest concentration at which an impact on any of the isotherms was observed and is significantly lower

than previously reported in the literature. Additionally, the effects are also studied as a function of concentration from this low value of 0.001 wt% up to 0.5 wt%. In all cases we seek to correlate structure and morphology changes to rheological parameters.

Chapter 2. Materials and methods

2.1. Materials

1,2-dipalmitoyl-sn-glycero-3-phosphocholine (DPPC), 1-palmitoyl-2oleoyl-sn-glycero-3-phosphoglycerol (POPG) and 1,2-dilauroyl-sn-glycero-3-phosphocholine (DLPC) were obtained in the powder form (Avanti Polar Lipids, Purity > 99%) and dissolved in chloroform (HPLC grade, Fisher Scientific) to make stock solutions. Ultrapure water (resistivity 18.2 M-Ω cm^{-1}) was obtained from an Easypure II LF purification system. Survanta and Infasurf was donated by Abbott Laboratories and Ony Inc, respectively. Levasil 200S (cationic), Bindzil 30/360 (anionic) and Bindzil 2034 DI (neutral) nanoparticles used for this research were provided by AkzoNobel and were supplied as aqueous suspensions.

2.2. Monolayer spreading solutions

The lipid mixtures were prepared by mixing aliquots of the stock chloroform solutions of DPPC, DLPC and/or POPG to obtain a molar ratio of 70:30. Infasurf were first lyophilized and then mixed with chloroform to obtain the desired concentration.

2.3. Subphase preparation and characterization

Nanoparticle suspensions were diluted with ultrapure water to obtain the desired nanoparticle concentration (given as weight %). The nanoparticle suspensions showed no significant surface activity (data not shown). The nanoparticle size and particle charge had been previously characterized using DLS and zeta potential using dispersions of the same concentrations as used in the experiments. Levasil (cationic) nanoparticles are 24 ± 7 nm in diameter and +42.8 ± 0.9 mV, Bindzil (anionic) nanoparticles are 17 ± 5 nm in diameter and -11.7 ± 4.1 mV and Bindzil DI (neutral) nanoparticles are 30 ± 10 nm in diameter and -35.0 ± 3.2 mV. When the neutral nanoparticles were first obtained from AkzoNobel they were neutral in charge but acquired an anionic charge over time. For this reason, the results from the neutral nanoparticles are only included in Appendix A rather than the main text. It should be noted that in all cases, the neutral nanoparticles behaviour was similar to that of the anionic nanoparticles.

2.4. Profile analysis tensiometer

Isotherms and rheology measurements were obtained using a pendant drop, profile analysis tensiometer (PAT). The PAT analyses the profile of the drop shape using the Young-Laplace equation to relate the curvature of the drop to an interfacial pressure value[83-86]. For obtaining isotherms using the PAT, model lung surfactant monolayers were spread on the surface of a 13 μL (corresponding surface area is 32 mm^2) drop of the subphase at the tip of a capillary. Spreading volumes ranged from 0.3 to 0.7 μL. Once the monolayer is spread on the drop surface, the surface area of the drop is increased to 40 mm^2 (26 μL) and was then allowed to equilibrate for 30 minutes. The waiting time also allowed the evaporation of chloroform from the surface of the subphase. Once the equilibration time was over, the drop area was adjusted to 40 mm^2 before compression was started. The monolayer is compressed due to the decrease in drop volume which is controlled by the micro-syringe pump at a pre-determined speed. The monolayer was compressed at a speed of 8 $Å^2$/molecule/minute until collapse to generate the isotherm. All isotherms were performed in at least duplicate and one representative isotherm is shown. The spreading error is approximately 7 ± 3 Å/molecule.

The monolayers for rheology measurements were prepared using the same method. For these measurement, a step through rheology (STR) program was used to obtain rheology measurements at different pressures using the same monolayer. Once the monolayer has been spread on the surface of the drop of water and allowed to equilibrate for the specified amount of time, the STR program was then started. The initial drop area is at 40 which is then compressed to 30 mm^2 at a compression speed of 8 $Å^2$/molecule/minute, the drop is then allowed to equilibrate for 300 seconds (5 mins) followed 600 seconds (10 mins) of sinusoidal oscillation of the drop area. Once the oscillations were complete, the drop was allowed to equilibrate for 300 seconds (5 minutes), followed by a small compression to increase the surface pressure by 2 – 3 mN/m, after which the drop was allowed to equilibrate for 300 seconds before the drop area underwent sinusoidal oscillations once again. This procedure was repeated to obtain rheology values for a pressure range of 10 – 55 mN/m for the same monolayer.

As the drop area is sinusoidally oscillated, the variation in surface pressure is recorded. The data obtained is then fitted using a Fourier transform after which the oscillations can be analyzed to

obtain viscosity and elasticity values at the specified surface pressure: the fitting procedure has been previously described [85].

As part of the data analysis procedure, each data point is evaluated and either retained or discarded based on the Total Harmonic Distortion (THD). The drop area was oscillated sinusoidally, therefore the surface pressure response is also sinusoidal in shape. The THD is a measure of how closely the oscillation data follows a reference sinusoidal shape; a lower THD implies a better fit. If the THD of the selected data point was lower than 15% then it was retained otherwise it was discarded. Thus, not all systems have an equivalent number of rheology data points.

Vrânceanu, Krägel and Wüstneck determined that the oscillation frequency of the drop should be such that it does not force the drop shape to deviate from its normal shape otherwise it will not fit to the Young-Laplace equation[83-85]. Moreover, the oscillation amplitude of the drop should always be kept below 10% of the actual drop area in order to prevent the drop shape deformation[87]. For our experiments the parameters chosen for frequency was 0.025 s^{-1} and the amplitude during oscillations was kept at 2.5% of the actual drop size in order to prevent drop shape deformation, early monolayer collapse and the drop falling off from the capillary. All rheology measurements are performed in duplicate and the data are presented as an overlay of two independent measurements, i.e. measurements on two independently prepared films. The "detachment pressure" for the PAT instrument refers to the pressure at which the drop detaches from the capillary.

2.5. Langmuir film balance

Traditionally surface pressure-area isotherms are generated using a Langmuir film balance. Moreover, it can be combined with optical imaging techniques as described below. For these measurements the subphase solution and monolayer solutions were prepared in the same manner as for pendant drop experiments, however, the spreading solution is 10-fold more concentrated. The monolayer film is spread at the air-water interface in the region between two moveable barriers and allowed to equilibrate as described in the previous section. To generate the isotherm, the two barriers are closed at 5 $Å^2$/molecule/minute which compresses the monolayer film.

Brewster angle microscopy (BAM) is used to image film morphology. P-polarized light is reflected at the water surface at the Brewster angle, the angle for total internal reflection. This angle is a function of the refractive indices of the two phases, in this case air and water. Upon spreading of an organic film at the air/water interface, the optical properties of the interface are altered and light is reflected. The different monolayer phases have different optical properties and generate different light intensities at the detector, thus enabling the observation of phase separation within the monolayer films.

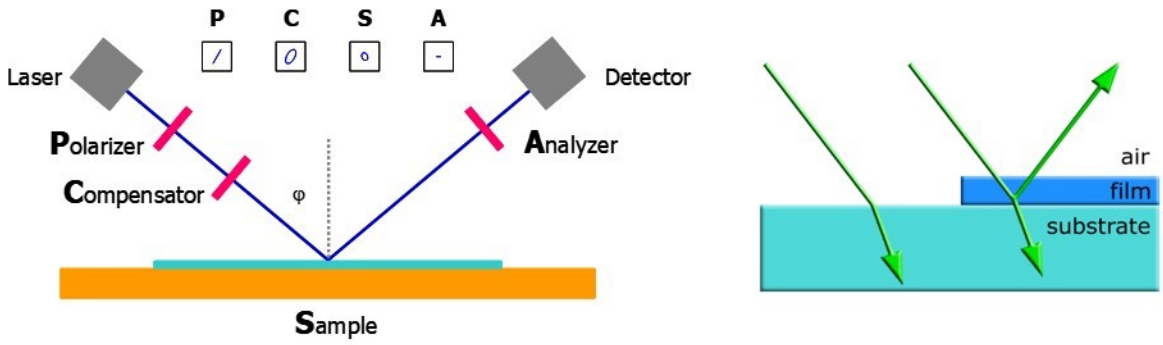

Figure 7. Schematic representation of Brewster angle microscopy.

These measurements were made using a custom Langmuir film balance (NIMA Technology) with a high aspect ratio (35 cm by 5 cm) that is coupled with an I-Elli2000 imaging ellipsometer (Nanofilm Technologies) comprising a 50 mW Nd:YAG laser (λ = 532 nm) and a 20x magnification lens set at an incident angle of 53.15°(the Brewster angle for an air/water interface).

2.6. Grazing incidence X-ray diffraction

In order to get a better understanding of how the nanoparticles are interacting with the model lung surfactant monolayer films, grazing incident X-ray diffraction (GIXD) experiments were performed at beamline 15-ID-C ChemMatCARS at the Advanced Photon Source (APS) in Argonne National Laboratory with the following parameters: x-ray beam wavelength of 1.239 Å, incident angle of 0.0906°, horizontal size of 20 µm, vertical size of 120 µm using gave a beam footprint of 20µm by 7.6 cm. The detector used was 2D Swiss Light source PILATUS 100K set to single-photon counting mode. Two sets of slits, one placed in front of the detector and the other placed 292.0 nm from the sample, where used to minimize intense low-angle scattering.

Experiments were done at the air-water interface of a 340 cm^2 Langmuir film, where the monolayer was spread and then compressed at a specified speed using a mobile barrier. The subphase solutions and monolayer solutions were made in the similar method as described for the BAM experiments. The data was analyzed using OriginPro 2016.

GIXD involves the use of x-rays from a synchrotron source at an angle of incidence below the critical angle for total reflection. Ordered arrays of molecules (in this case the all-trans, fully extended chains of the condensed phase) will give rise to diffraction peaks. All diffraction peaks are analyzed as a function of the in-plane (Q_{xy}) and out-of-plane (Q_z) diffraction components which yield information on the lattice parameters and molecular tilt angles and direction. It is important to note that only condensed phase lipids will give rise to diffraction peaks. The peak position in Q_{xy} yields the unit cell spacings while the position in Q_z yields the tilt angle of the lipid chains; the full width at half maximum (FWHM) in Q_{xy} provides information on the crystallinity (referred to as the coherence length, l_c) of the ordered phase. The FWHM in Qz correlates to the length (L) of the scattering rod (alkyl chain thickness). The formulas for calculation of these parameters are[88]:

$$d = (2 \times \pi) / \Delta q_{xy} \quad \text{and} \quad l_c = ((2 \times \pi) / \Delta q_{xy}) \times 0.9$$

$$L = 0.9 \times ((2 \times \pi) / FWHM_{Qz})$$

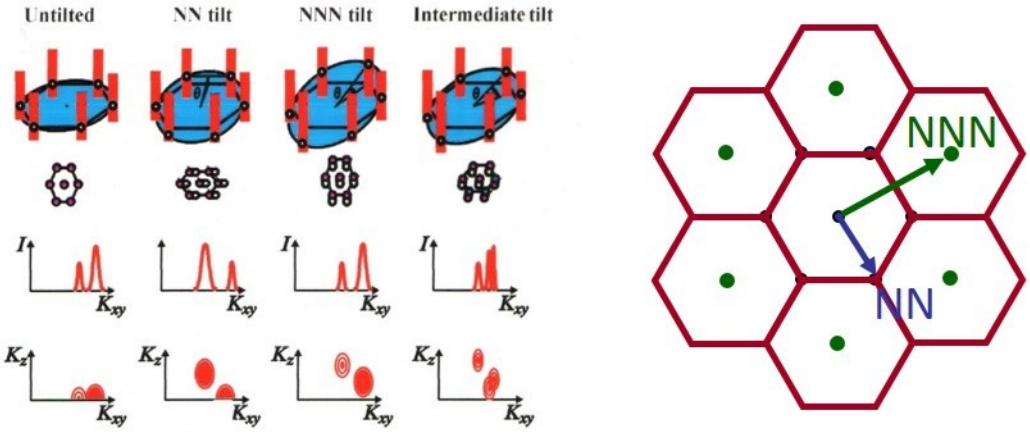

Figure 8. Schematic of Grazing incidence diffraction and possible tilt angles[89]. Adapted from O'Flaherty *et al.* Langmuir, 2005, 21, 11161-11166.

Chapter 3. Impact of charged silica nanoparticles on model lung surfactant systems

Section 3.1 and 3.2 focus on the characterization of the four model membranes and the impact of low concentrations of charged silica nanoparticles dispersed in the subphase. Only the results for anionic and cationic silica nanoparticles are shown as the "neutral" nanoparticles had acquired a negative charge at the time these experiments were carried out. For completeness, the data for the same systems on subphases containing neutral nanoparticles are included in Appendix A. Grazing Incidence X-ray Diffraction data is included for the DPPC, 70:30 DPPC:DLPC and 70:30 DPPC:POPG systems. Postdoctoral fellow, Shirin Behyan, guided the analysis and interpretation of the GIXD data that has been published as Nanoparticle-Induced Structural Changes in Lung Surfactant Membranes: An X-ray Scattering Study, Shirin Behyan, Olga Borozenko, Abdullah Khan, Manon Faral, Antonella Badia and Christine E. DeWolf Environmental Science: Nano, 2018, DOI: 10.1039/C8EN00189H.

3.1. Characterization of the model membranes

The surface pressure-area isotherms obtained using the pendant drop tensiometer for the four systems, DPPC, 70:30 DPPC:DLPC, 70:30 DPPC:POPG and Infasurf on water, are shown in Figure 9. All isotherms are in good agreement with the literature[73,90-92]. In order to obtain the isotherm, the lipid film is spread on a pendant drop and the drop area is reduced. The maximum pressure that can be obtained with this method is limited as the drop detaches from the capillary at very small drop volumes. The expanded nature of these films generates isotherms that occur over a large range of molecular areas, thus drop detachment occurs before film collapse would normally be observed using a traditional Langmuir film balance.

For the single component (DPPC) film, the liquid-expanded to condensed (LE-C) phase transition, takes place around 10 mN/m and is exhibited as a horizontal plateau in the isotherm. Over the phase transition the relative proportions of these two phases (LE and C) change until the film is fully condensed in a tilted phase, as it already is well established. In the case of the binary lipid mixtures, the phase transition is less sharp and is shifted to a higher surface pressure, around 17 mN/m. The POPG lipid has one unsaturated chain and the presence of the double bond in one of the alkyl chains hinders it from forming a condensed phase at room temperature,

therefore, stays in the LE phase until collapse. Although DLPC is a disaturated lipid, the relatively short tails only have 12 carbons, which is not long enough for it to form condensed phase at room temperature and therefore the isotherm of a DLPC film will also remain in the LE phase until collapse. The main phase transition temperature (T_m) for both POPG and DLPC is -2°C[93]. A squeeze-out of the LE phase at higher pressures has been reported for such phase separated binary mixtures (often observed as a second plateau) as the LE phase has a lower collapse pressure. This is then followed by an increase in pressure for the remaining condensed phase components which are stable to much higher surface pressures (lower surface tensions)[73]. This was not observed but such transitions can be difficult to obtain on a drop tensiometer with the much smaller surface areas and low drop stability at small drop areas/volumes.

Infasurf not only has a mixture of saturated and unsaturated lipids but it also contains the surfactant proteins SP-B and SP-C; the phase transition is no longer visible in the isotherms despite phase separation occurring due to the complexity of the mixture (a mixture of chain lengths, degrees of saturation and headgroups for the lipids)[73]. Additionally, the proteins maintain some LE phase even with squeeze-out and reservoir formation (associated with the plateau at 45 mN/m)[65]. It should be noted that the molecular areas reported for Infasurf in the isotherms are arbitrary values since the exact composition is not known. For comparison to the well-defined lipid only systems, the amount of Infasurf spread was adjusted to yield a similar critical area. After the squeeze-out, the pressure begins to increase again, although it is not possible to compress until collapse with the pendant drop.

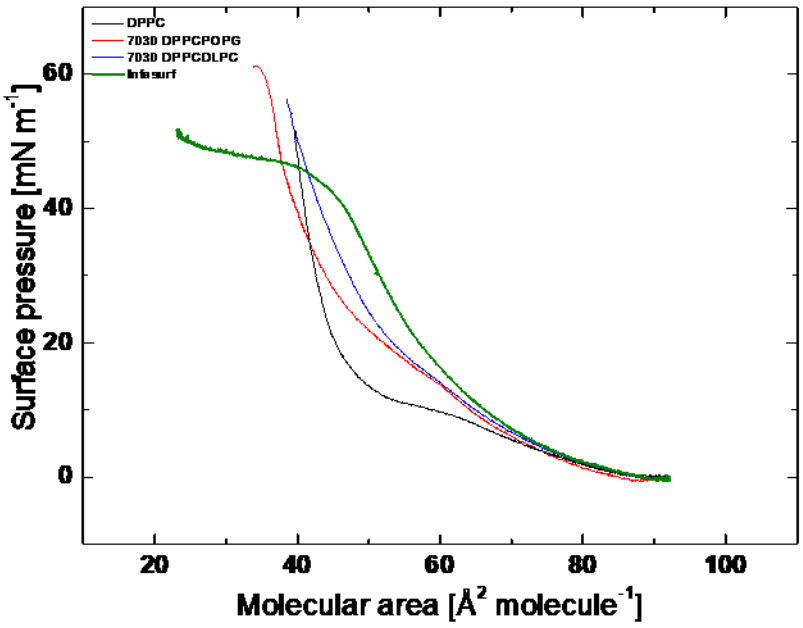

Figure 9. Surface pressure-area isotherms of the four model membranes on a water subphase at room temperature. Note that the molecular area for Infasurf is arbitrary as the molecular weight for this natural extract is not known.

Figure 10 shows the viscosity and elasticity data for the four different systems on a water subphase. DPPC exhibits the highest viscosity and elasticity values compared to the other three systems at moderate to high pressures. Anton *et al*. have compared six different lipids, with varying head groups, lipid chain length and units of saturation in lipid chains, and have found that viscosity is mainly dominated by head group interactions between neighboring lipids and with the subphase. On the other hand, elasticity is regulated by lipid chain interactions and lipid phase. Saturated lipids that form condensed phases have higher elasticity than unsaturated lipids, where the units of unsaturation decrease the chain ordering and packing. Furthermore, units of unsaturation decrease lipid chain interaction which results in lower elasticity[70]. DPPC headgroup is zwitterionic compared to POPG headgroup which has an overall negative charge. There is charge repulsion between headgroups, which creates a larger distance between them and therefore lowers possible hydrogen bonding between headgroups as demonstrated by Pimthon *et al*.[94].

For all four systems, very low viscosities are observed at low pressures when the film is in a LE phase, until the onset of domain formation, which is usually observed even before the surface pressure is registered as a plateau in the isotherm. For DPPC, condensed phase domains begin to appear around 5 mN/m and these begin to coalesce above 10 mN/m[73]. The viscosity increases with increasing proportion of condensed phase domains until coalescence at which point there is a distinct change in slope. This slope above 10 mN/m correlates to the viscosity values for a condensed phase with a slope representative of the change in chain tilt angle due to compression[73].

For DPPC:POPG and DPPC:DLPC, the isotherms showed a broadening of the phase transition over a larger range of surface pressures, a trend also evident in the viscosity and elasticity data. One significant difference between the two is the behaviour at higher surface pressures. For the DPPC:DLPC system, the DLPC-rich LE phase is more stable and persists to higher surface pressures[90], correlating with the low slope in viscosity and near constant elasticity values above 20 mN/m. Nojima and Iwata estimated the viscosity inside lipid bilayers formed by different phosphatidylcholines and demonstrated that despite both DPPC and DLPC being saturated lipids, DPPC has a significantly higher viscosity than DLPC due to the phase formed[95]. On the other hand, the POPG-rich LE phase is less stable and begins to be squeezed out at lower pressures, leading to values that begin to move towards those of pure DPPC[70]. By 40 mN/m the POPG LE phase appears to be fully squeezed out of the surface[96].

Infasurf exhibits a fairly small increase in viscosity and elasticity and maintains those values throughout the pressure range, moreover, it has the lowest viscosity and elasticity values compared to the other systems. With the large mixture of chain lengths and degrees of saturation, domain formation begins below 5 mN/m, domain sizes are variable with co-existing micron and nanometer sized domains and there is a significant proportion of LE phase at all pressures, all giving rise to the long continuous increase in viscosity[96].

These differences are mirrored in the elasticity measurements. There is a distinct change in slope with the onset of domain coalescence. For DPPC, which exhibits full coalescence, the elasticity continues to increase as the film is compressed, while for the other systems, in which a LE phase is present, the elasticity is dominated by this phase and plateaus once all of the condensed phase

is formed (with the exception of DPPC:POPG which shows a second increase as the LE phase is squeezed out and eventually reaches values similar to DPPC upon full coalescence, whereas DLPC is stable to much higher surface pressures). For Infasurf, these results are consistent with one of the reported roles of the surface active proteins SP-B and SP-C, namely to moderate viscosity and elasticity and maintain fluid phase at the interface until the film is collapsed[50].

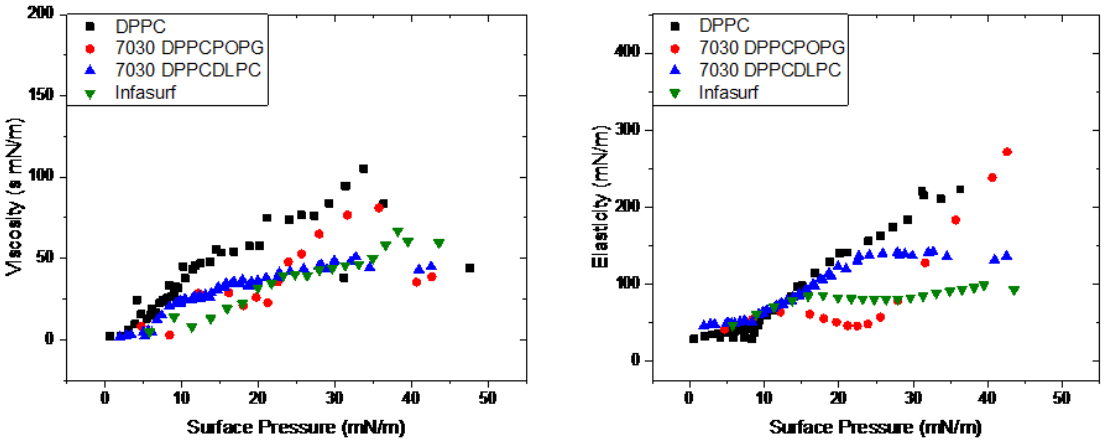

Figure 10. Viscoelasticity measurements of the four model membranes on a water subphase at room temperature. Each data set comprises duplicate measurements made on two, independently prepared films.

3.2. Impact of low concentrations of silica nanoparticles on lung surfactant model membranes

The impact of low concentrations of charged silica nanoparticles on the four model membranes was studied via their impact on the surface pressure-area isotherms, surface rheology and condensed phase structure.

3.2.1. Isotherms for model membranes spread on silica nanoparticle subphases

The impact of 0.001 wt% cationic and anionic silica nanoparticles on the surface pressure-area isotherms of the four model membranes are shown in Figure 11.

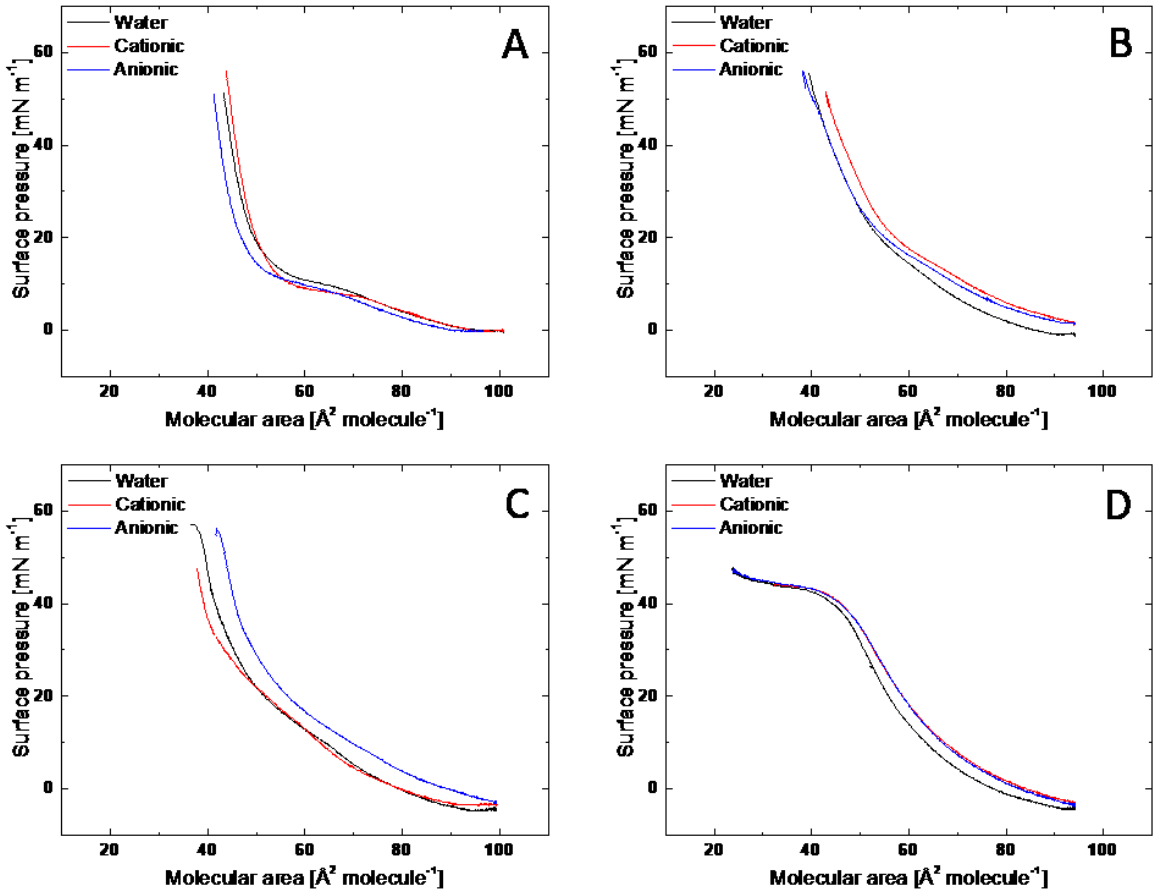

Figure 11. Surface pressure-area isotherms of each of the model membrane systems (A: DPPC, B: DPPC:DLPC, C: DPPC:POPG, D: Infasurf) spread on the three subphases (water: black, 0.001 wt% cationic silica nanoparticles: red, 0.001 wt% anionic silica nanoparticles: blue) at room temperature.

For three systems, DPPC, DPPC:DLPC and Infasurf, the isotherms are all very similar to each other in shape with only slight changes in the area per molecule in the presence of 0.001 wt% charged silica nanoparticles. On the other hand, the nanoparticles have a larger impact on the DPPC:POPG system with the negatively charged film that comprises a highly negatively charged POPG-rich LE phase and slightly negatively charged DPPC-rich condensed phase. Despite the negative charge, the cationic nanoparticles appear to have a minimal impact on the molecular area. On the other hand, the anionic nanoparticles induce a shift to higher molecular areas (the Bindzil DI nanoparticles, induce an even larger shift to higher molecular areas when they are

negatively charged as shown in Appendix A). The anionic nanoparticles may preferentially interact with the positive charge of the zwitterionic choline headgroup inducing either a change in the orientation of the lipid in this phase or inducing repulsion between the adsorbed anionic nanoparticles and the surrounding highly anionic LE phase.

The presence of nanoparticles not only causes changes in isotherm but also affects the domain morphology of the lipid film. McConnell and McConlogue *et al*., have shown that in water DPPC domain morphology are bean shaped but Chakraborty *et al*. have shown that in the presence of 1 wt% anionic, hydrophobic nanodiamonds that are co-spread with the lipids, the shape is altered. For DPPC, the domains no longer maintain their characteristic bean-shape but adopt a more stretched out spiral structure. The change in domain shape observed by them indicates a lowering of the line tension between the LC domains and LE area[92,97,98]. This effect was also observed for a 70:30 DPPC:POPG lipid film, attributed to the preferential interaction of the nanodiamonds with the LC DPPC domains while avoiding the fluid POPG phase[98]. Unusually, they reported no change in the isotherms despite the incorporation of a hydrophobic nanoparticle and despite the additional charge-charge repulsion between the anionic nanoparticles and anionic LE phase. One might also expect an expansion for Infasurf which contains a significant proportion of anionic lipids, however, the cationic proteins (SP-B) can shield the anionic lipid from the impact of charged species in the subphase, thus limiting the isotherm changes due to the adsorption of the nanoparticles[96].

3.2.2. Rheological data for model membranes spread on silica nanoparticle subphases

The rheology data for DPPC on all three subphases, i.e. the absence of nanoparticles (water subphase) and the presence of 0.001 wt% cationic or anionic silica nanoparticles are shown in Figure 12. In agreement with the isotherms, the slight differences in the plateau pressures are reflected in the viscosity and elasticity data. In the LE phase, the DPPC rheology is unaffected by the presence of the nanoparticles but the behaviour differs above the phase transition. DPPC has high viscosity values in the absence of nanoparticles. The presence of either cationic or anionic nanoparticles induce a significant decrease in viscosity. Given this behaviour is reminiscent of the plateau in viscosity observed with mixed lipid systems, it is tempting to attribute this behaviour to the presence of a LE phase, however Brewster angle microscopy imaging (data not

shown) confirms that the film is a homogeneous condensed phase on the micron scale. Viscosity, the resistance to flow, is associated with head group-head group and head-group subphase interactions and these are clearly disrupted in the condensed phase in the presence of particles. Similarly, the DPPC elasticity appears only to be affected by the presence of nanoparticles at surface pressures above the phase transition pressure. Unlike the viscosity, the presence of nanoparticles induces a distinct increase in elasticity. Again, the impact was the same irrespective of the nanoparticle type present. Elasticity represents the stress/strain relationship for the film (the force or stress required to produce a change in area or strain). Thus a high elasticity implies a low deformation for a given stress. It is also related to the change in surface tension with respect to a change in area. In the condensed phase, the presence of any particles in the subphase appears to generically increase the film's resistance to deformation, which may be related to the size of the particle (a rough area calculation would suggest that each adsorbed nanoparticle would interact with hundreds of lipids).

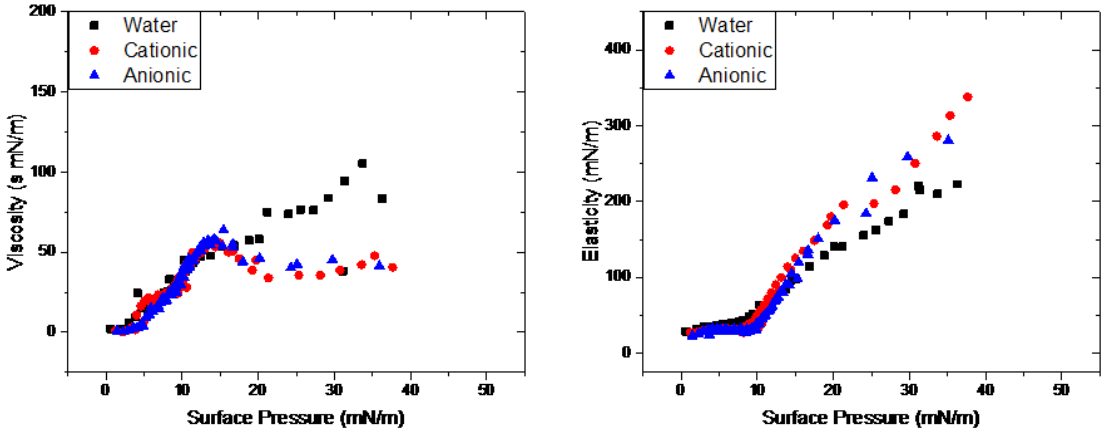

Figure 12. Viscoelasticity measurements of DPPC monolayers spread on different subphases at room temperature: water (black), 0.001 wt% cationic silica nanoparticles (red) and 0.001 wt% anionic silica nanoparticles (blue). Each data set comprises duplicate measurements made on two, independently prepared films.

With the phase separated, binary lipid systems (Figures 13 and 14), the impact of the nanoparticles on the viscosity and elasticity reflects the differences in the isotherm and the surface pressures at which phase transitions occur much more than the magnitude of the values

attained, i.e. the same viscosity/elasticity-surface pressure relationship with a shift to higher surface pressures. For DPPC:DLPC it was noted in section 3.1 that the increase in viscosity and elasticity above the phase transition were moderated in these systems due to the continuous presence of LE phase. The viscosity appears to show a step-change immediately after condensed phase domains begin to appear, whereas the elasticity shows a continuous change over the phase transition and levels out only after the end of the phase transition region. The only discernable difference in the magnitude of the viscosity in the presence of nanoparticles (Figure 13) occurs after the phase transition and again both nanoparticle types induce a decrease in viscosity, albeit much smaller as the viscosity is already lower. This time there is no apparent change in elasticity after the phase transition, attributed to the presence of the LE phase. The film elasticity is dominated by the properties of the LE phase that are already lower than the C phase, therefore lessening the impact of the nanoparticles. It should be noted that the anionic nanoparticles show a shift of the phase transition to higher surface pressures that is more prominent in the rheological data than the isotherms.

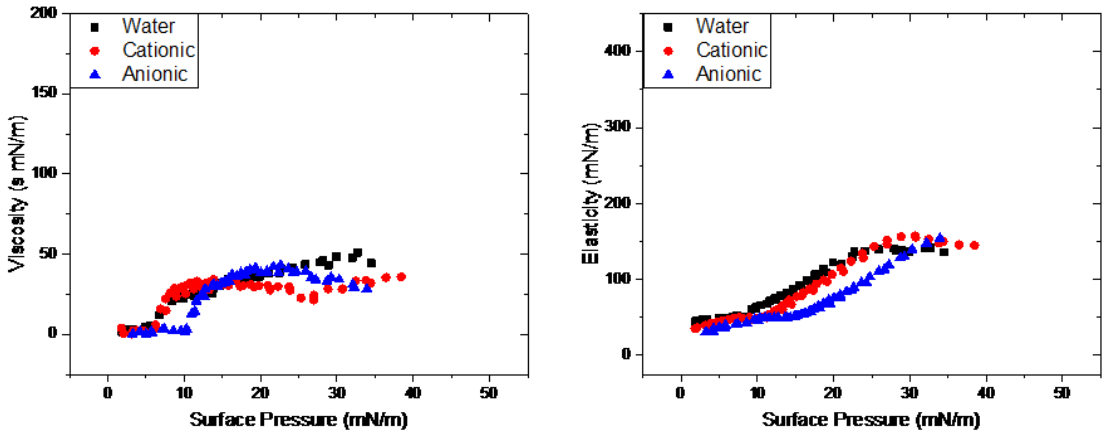

Figure 13. Viscoelasticity measurements of 70:30 DPPC:DLPC monolayers spread on different subphases at room temperature: water (black), 0.001 wt% cationic silica nanoparticles (red) and 0.001 wt% anionic silica nanoparticles (blue). Each data set comprises duplicate measurements made on two, independently prepared films.

The interaction of nanoparticles with the DPPC:POPG monolayer produces a similar trend. Again, there is little impact of the nanoparticles on viscosity or elasticity at low pressure, when

all components are in a LE phase (Figure 14). The phase transition is much more prominent in both the viscosity and elasticity data, perhaps due to the separation into two phases of distinct charge and/or headgroup. It was anticipated that the cationic particles would be attracted to the POPG causing a large impact on viscosity and elasticity, which was not observed. Similarly, despite large changes in the isotherm position, it seems the net elasticity of the films, dominated by the presence of a fluid phase, is unaffected. The impact of particles appears only above 30 mN/m, i.e. at pressures where the anionic POPG is thought to be squeezing-out of the film. At these higher pressures an increase in viscosity is observed in the presence of anionic particles. As discussed earlier, it is likely that the anionic nanoparticles are interacting with the DPPC-rich condensed phase rather than the POPG-rich LE phase. The anionic nanoparticles adsorbed on the condensed phase cause a repulsion between islands and matrix, increasing the viscosity for this system. Such a repulsion would not be observed when the LE-phase is zwitterionic (DPPC:DLPC) or when there is no LE phase (DPPC).

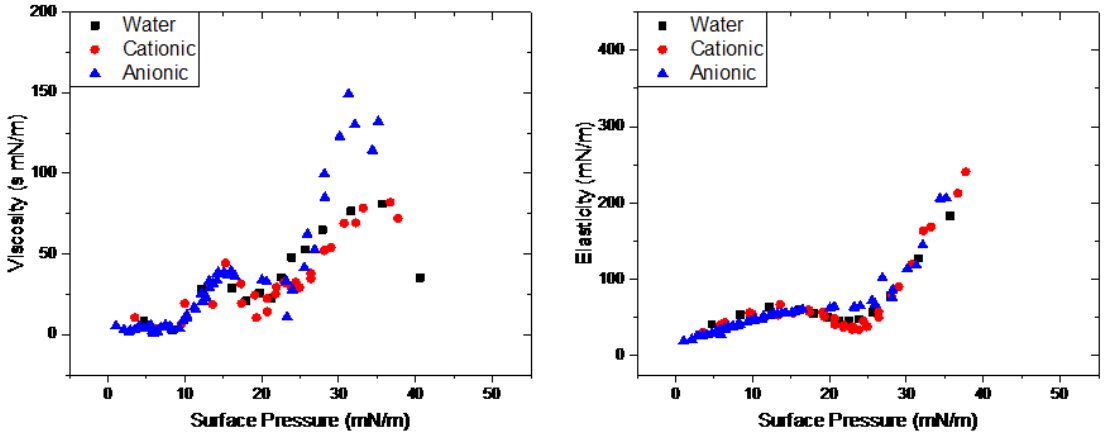

Figure 14. Viscoelasticity measurements of 70:30 DPPC:POPG monolayers spread on different subphases at room temperature: water (black), 0.001 wt% cationic silica nanoparticles (red) and 0.001 wt% anionic silica nanoparticles (blue). Each data set comprises duplicate measurements made on two, independently prepared films.

Finally, the anionic nanoparticles cause a similar impact on Infasurf as was observed with DPPC:POPG, namely an increase in viscosity above 30 mN/m and increase in elasticity over the course of the phase transition (Figure 15). Although the effects may appear subtle, at the point of

the largest difference between the absence and presence of nanoparticles, namely in the middle of the phase transition, the elasticity is increased by approximately 31%. The range of pressures over which the elasticity is increased is greater for Infasurf, in agreement with a broad phase transition due to the complexity of the composition of this multicomponent mixture. Given the pendant drop cannot reach the pressures high enough for significant reservoir formation, it is not clear what impact the nanoparticles will have on this process.

In all cases the Bindzil DI nanoparticles, which actually carry higher charge density than the anionic Bindzil nanoparticles show the same effect but significantly more pronounced, highlighting that the charge density plays an important role in determining the extent of impact (see Appendix A).

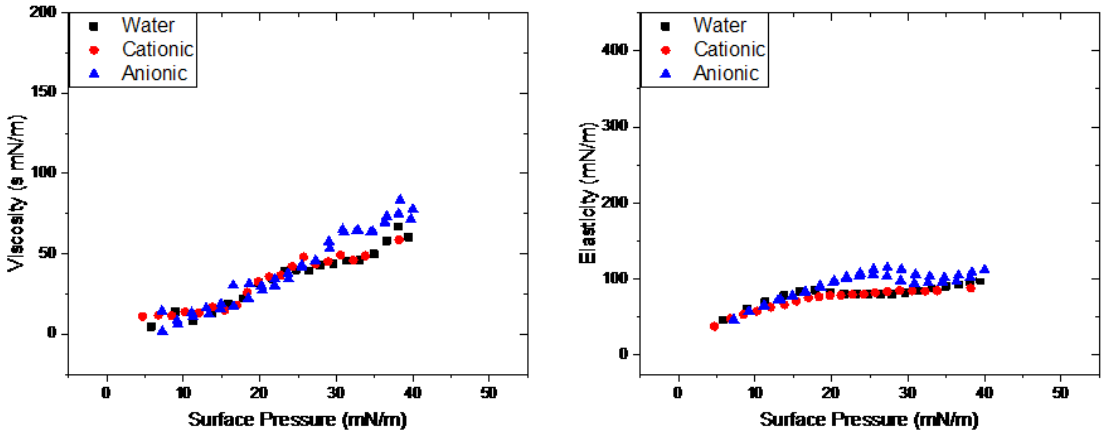

Figure 15. Viscoelasticity measurements of Infasurf monolayers spread on different subphases at room temperature: water (black), 0.001 wt% cationic silica nanoparticles (red) and 0.001 wt% anionic silica nanoparticles (blue). Each data set comprises duplicate measurements made on two, independently prepared films.

3.2.3. Structural analysis of model membranes spread on silica nanoparticle subphases

As mentioned earlier, GIXD diffraction peaks are only observed when there is an ordered surface phase present. A surface pressure of 35 mN/m was chosen to ensure all systems had phase

separated but that squeeze-out and reservoir formation had not yet taken place. GIXD was used to assess the impact of the nanoparticles on the lateral lipid structure within the condensed phase.

Figure 16 shows the GIXD images of the DPPC monolayer in the presence and absence of 0.001 wt% cationic and anionic nanoparticles. The presence of out-of-plane peaks (i.e. peaks with a center at $Q_z>0$) indicate that there is a tilt in the lipid chains. The sharpness of the peaks is an indication of the crystallinity of the condensed phase: the sharper the peaks the more crystalline or ordered the surface phase. In agreement with the literature, DPPC exhibits three peaks, all at $Q_z>0$, indicative of an oblique lattice with an intermediate tilt, i.e. between Nearest Neighbour (NN) and Next Nearest Neighbour (NNN)[99]. The calculated tilt angle of the lipid chains (27.1°) is also in agreement to that reported in literature[99]. For all three types of subphases, no change is observed for the unit cell since the tilt of the alkyl chains are between that of NN and NNN (Table 1). The presence of nanoparticles induces a slight increase in alkyl chain tilt angles (Table 1), which may be caused by lipid headgroup reorientation due to the presence and interaction with the charged nanoparticles[100,101].

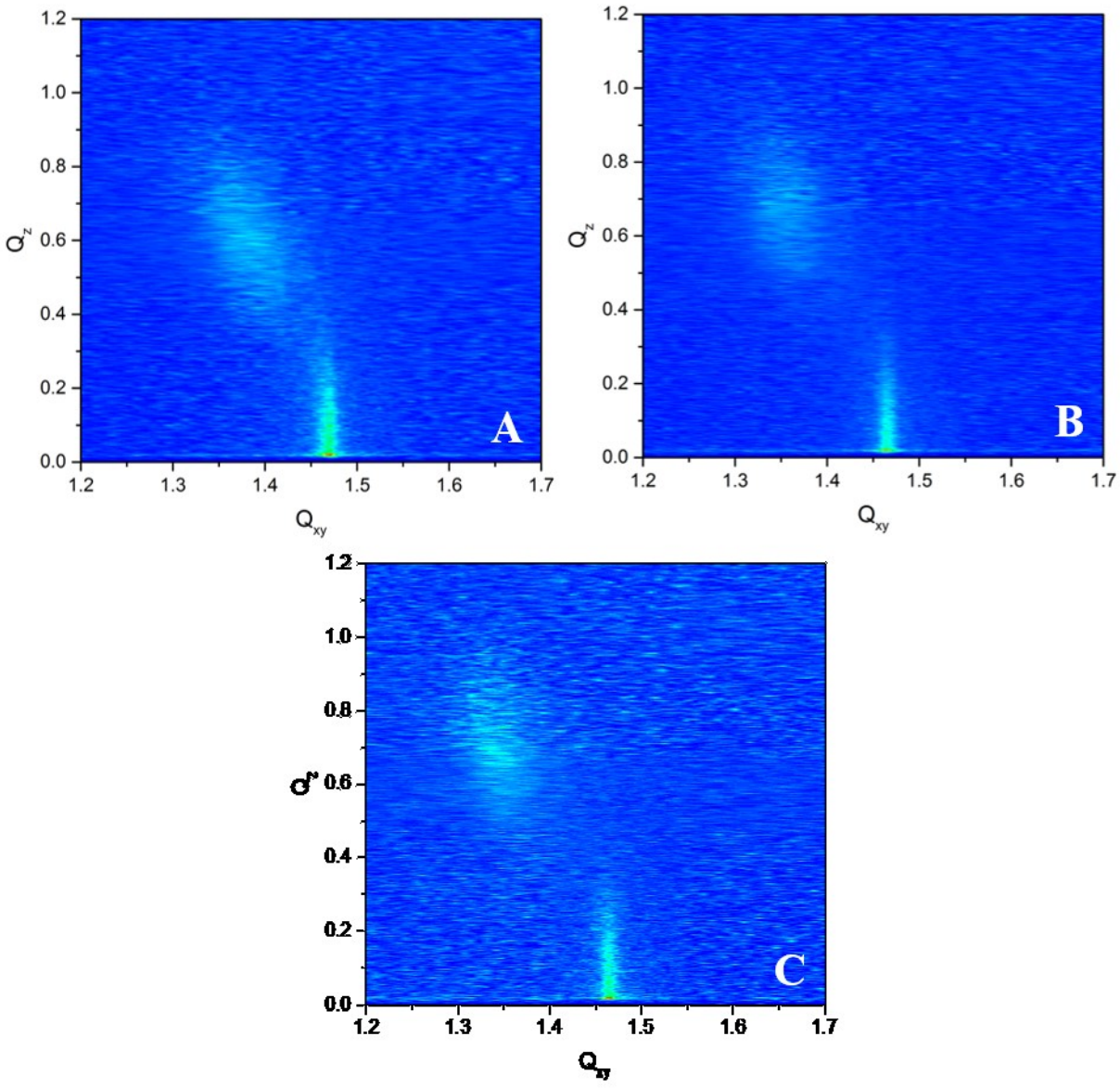

Figure 16. GIXD intensity as a function of the in-plane (Q_{xy}) and out-of-plane (Q_z) components of the scattering vector for a DPPC monolayer at 35 mN/m in water (A) 0.001 wt% cationic nanoparticles (B) and 0.001% anionic nanoparticles (C).

Table 1. Summary of lattice type, tilt azimuth and tilt angles measured by GIXD for DPPC monolayers.

System		π (mN/m)	Lattice	Tilt Azimuth	Tilt Angle (°)
DPPC	Water	35	Oblique	Intermediate	27.1
	Cationic	35	Oblique	Intermediate	31.3
	Anionic	35	Oblique	Intermediate	32.7

Figure 17 shows the GIXD images of the 70:30 DPPC:DLPC monolayer in the presence and absence of 0.001 wt% cationic and anionic nanoparticles. Once again, the presence of out-of-plane peaks are indicative of lipid chain tilt. DPPC and DLPC share the same headgroup but differ in lipid chain lengths. Due to the shorter lipid chains, a pure DLPC monolayer is unable to reach C phase and stays in the LE phase till film collapse. However, this monolayer has been reported to show phase separation with partial miscibility[102]. Therefore, it is possible that mixing DPPC with DLPC (70:30 ratio) causes the resulting monolayer to have a reduced amount of condensed phase and as a result the diffraction peaks have significantly lower intensity and a higher background noise is observed (Figure 17) compared to the DPPC monolayers (Figure 16). The alkyl chain tilt angle in water subphase for the mixed monolayer (28.4°) is larger than that of DPPC in water subphase (27.1°) which is most likely due to the presence of the short chain DLPC incorporated into the DPPC condensed phase. Similarly to DPPC monolayer, the 70:30 DPPC:DLPC monolayer also has an oblique unit cell in all three types of subphase with very little change in alkyl chain tilt, where the changes can be attributed to lipid headgroup reorientation due to their interaction with the charged nanoparticles. Unlike the DPPC monolayer, in the presence of anionic nanoparticles for the mixture there is a decrease in tilt angle and this may be due to the DLPC being incorporated in the condensed phase monolayer (Table 2).

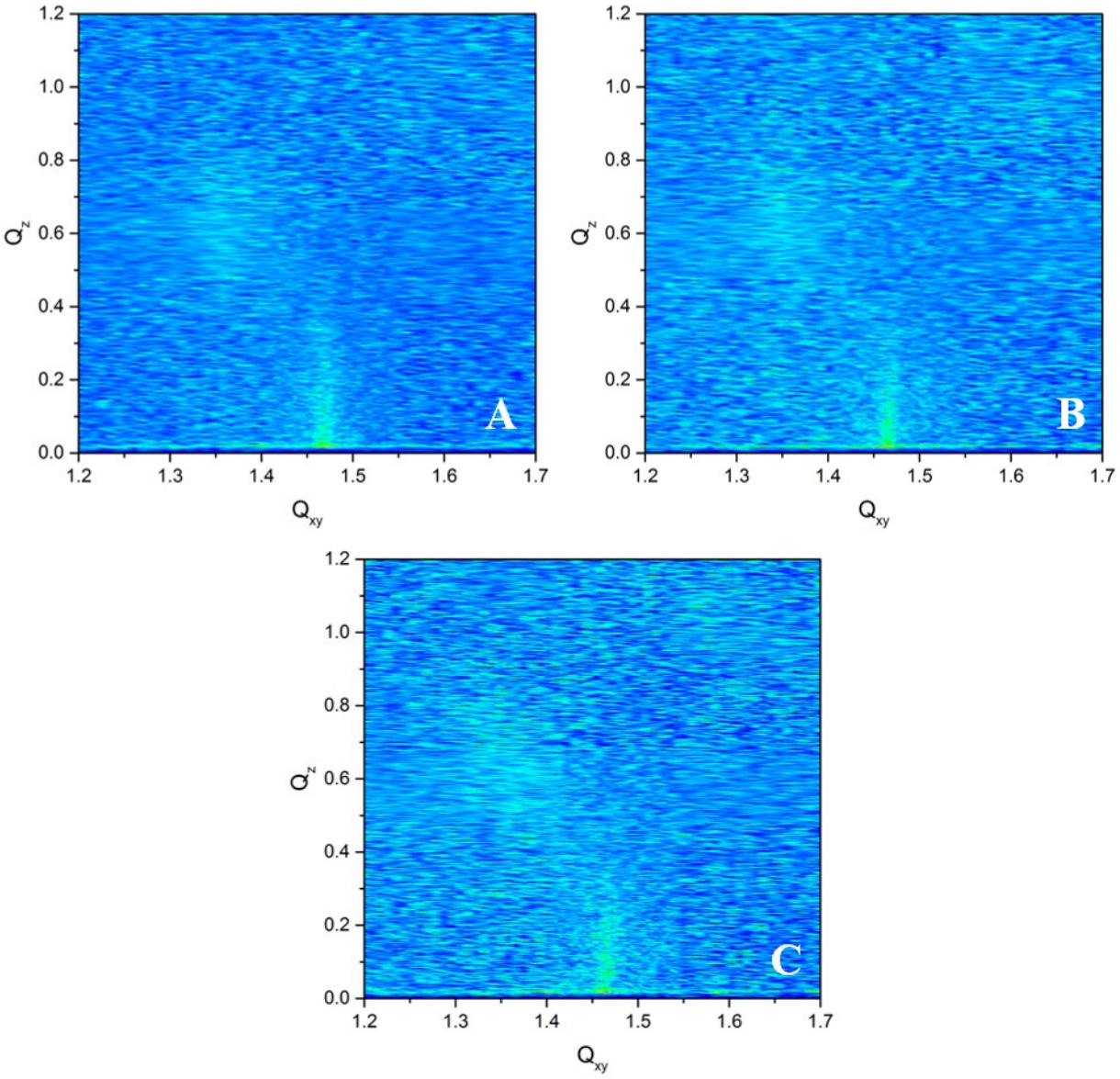

Figure 17. GIXD intensity as a function of the in-plane (Q_{xy}) and out-of-plane (Q_z) components of the scattering vector for a 70:30 DPPC:DLPC monolayer at 35 mN/m in water (A) 0.001 wt% cationic nanoparticles (B) and 0.001% anionic nanoparticles (C).

Table 2. Summary of lattice type, tilt azimuth and tilt angles measured by GIXD for 70:30 DPPC:DLPC monolayers.

System		π (mN/m)	Lattice	Tilt Azimuth	Tilt Angle (°)
70:30 DPPC:DLPC	Water	35	Oblique	Intermediate	28.4
	Cationic	35	Oblique	Intermediate	28.4
	Anionic	35	Oblique	Intermediate	26.7

Figure 18 shows the GIXD images of 70:30 DPPC:POPG monolayer in the presence and absence of 0.001 wt% cationic and anionic nanoparticles. Contrary to GIXD images for the 70:30 DPPC:DLPC monolayer (Figure 17) there is significantly less background noise for the 70:30 DPPC:POPG monolayer (Figure 18) indicating that the intensity of diffraction is higher since there is more condensed phase present in the monolayer. The three diffraction peaks (Figure 18) and an oblique unit cell (Table 3) observed are in agreement with the literature for this monolayer, however the lipid tilt angle is decreased (Table 3)[68]. Bringezu *et al*. have reported that POPG can partially incorporate into the DPPC condensed phase and since the size of POPG headgroup is smaller than that of DPPC this mixed condensed phase has a tighter packing of headgroups which results in a lower tilt angle[68]. Similar to the two previous systems, DPPC and 70:30 DPPC:DLPC, an oblique unit cell is observed for water and anionic nanoparticle subphase with little change in the lipid chain tilt angle. Unlike the previous two lipid systems, the presence of cationic nanoparticles induces a significant change in the unit cell and lipid chain tilt angle. The calculated tilt angle for the lipid chains in the presence of cationic nanoparticles is 6.8° and the unit cell is centered rectangular (Table 3), such low tilt angles have been observed in the presence of chaotropic agents that disturb the hydrogen bonding network [103]. Since such a drastic change in tilt angle was not observed with DPPC monolayer in the presence of cationic nanoparticles, the change can be attributed to the presence of anionic POPG present in the DPPC condensed phase domains, which interacts strongly with the cationic nanoparticles.

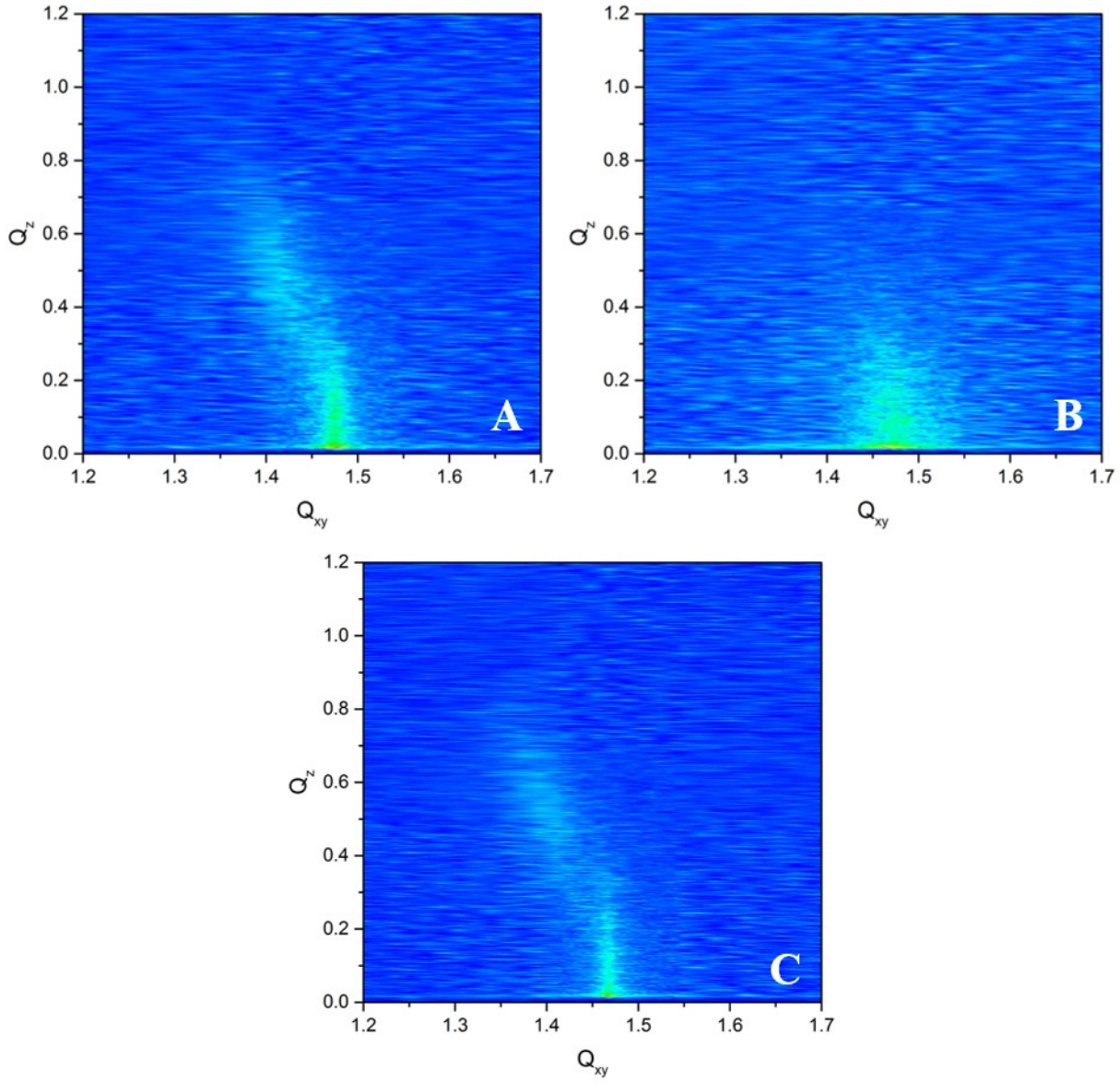

Figure 18. GIXD intensity as a function of the in-plane (Q_{xy}) and out-of-plane (Q_z) components of the scattering vector for a 70:30 DPPC:POPG monolayer at 35 mN/m in water (A) 0.001 wt% cationic nanoparticles (B) and 0.001% anionic nanoparticles (C).

Table 3. Summary of lattice type, tilt azimuth and tilt angles measured by GIXD for 70:30 DPPC:POPG monolayers.

System		π (mN/m)	Lattice	Tilt Azimuth	Tilt Angle (°)
70:30 DPPC:POPG	Water	35	Oblique	Intermediate	20.0
	Cationic	35	Centered Rectangular	NNN	6.8
	Anionic	35	Oblique	Intermediate	22.7

GIXD data was also obtained for Infasurf monolayers (Appendix B) but the complex lipid composition yields multiple phases such that a definitive fit could not be obtained. Qualitatively, the effects are similar to those observed with DPPC:POPG, namely a slight expansion of the unit cell in the presence of anionic nanoparticles and a reduction in title angle in the presence of cationic nanoparticles.

3.3. Concentration studies on model membranes

In section 3.2 it was shown that low concentrations of nanoparticles can impact the physicochemical properties of the model lung surfactant films. In order to determine the impact of nanoparticle concentration, studies were performed with the two model systems that best represented the lung surfactant, 70:30 DPPC:POPG (lipid-only system with the charged LE phase) and Infasurf (lipid-protein system), with concentrations ranging from 0.001 wt% to 0.5 wt%. In order to ensure equilibration at each concentration of dispersed nanoparticles in the subphase, films were all allowed to equilibrate for 30 minutes prior to performing isotherms and rheology experiments. In order to control the lipid:nanoparticle ratio (200:1), the same amount of lipid was always spread on the surface of a 40 mm^2 drop and the NP concentration was varied. As a result, if the nanoparticle induces a film expansion, the shift can be sufficiently large such that a gaseous phase cannot be observed.

3.3.1. Impact of cationic nanoparticles as a function of concentration

The surface pressure-area isotherms for 70:30 DPPC:POPG and Infasurf on water with increasing concentrations (given as wt% of subphase) of cationic silica nanoparticles obtained with the pendant drop tensiometer are shown in Figure 19. In all of the DPPC:POPG isotherms, the LE-C phase transition starting around 10 mN/m is visible. With increasing concentration of cationic nanoparticles in the subphase the isotherm is shifted to higher molecular areas suggesting that increasingly more nanoparticles are attracted to the anionic lipid film. However, it must be noted that the shift in molecular area does not scale linearly with nanoparticle concentration. In particular the isotherms for 0.01 wt% and 0.1 wt% Levasil are, within experimental error, identical. Notably there is a distinct shape change in addition to a shift to higher molecular areas at 0.5 wt% cationic nanoparticles and a much lower collapse (the film pressure begins to plateau and drop at 50 mN/m). These suggest that there may be a point at which the film is saturated with adsorbed nanoparticles and begins to exhibit behaviour of a nanoparticle film rather that a lipid film. Shifts to higher molecular areas are also observed for cationic nanoparticles interacting with Infasurf but the shifts are much smaller, indicating that the presence of the cationic protein SP-B reduces the net attraction of the cationic nanoparticles to the surface. This is in agreement with previous findings that the SP-B can screen counterions and other charged species from the surface[96]. Despite the smaller shift, again 0.5 wt% has a clear impact near the squeeze-out pressure of 50 mN/m and alters this squeeze-out plateau, suggesting that such a high concentration of nanoparticles in the subphase alters the squeeze-out process and may alter the film buckling process and mechanism. In the absence of surfactant proteins, lipid films collapse via a fracture mechanism while in the presence of the surfactant proteins this is modified to a folding process[52]. The cationic nanoparticles may either interfere with the ability of the proteins to carry out their function or the particles themselves may facilitate collapse via a different mechanism.

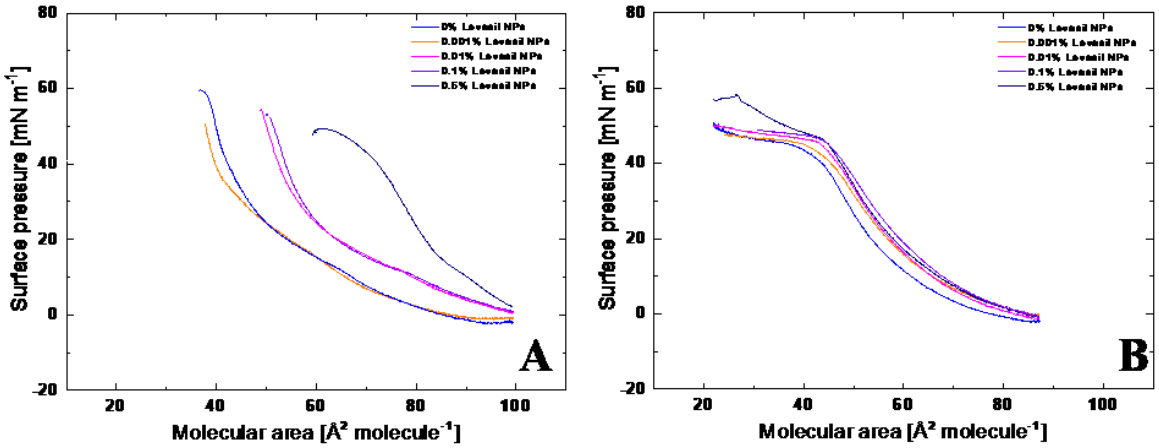

Figure 19. Surface pressure–area isotherms of 70:30 DPPC:POPG (A) and Infasurf (B) monolayers in cationic nanoparticles with increasing particle concentration at room temperature.

The viscosity and elasticity data for the two films in the presence of varying concentrations of nanoparticles are shown in Figure 20. The features of the viscosity versus surface pressure and elasticity versus surface pressure were describe in the previous chapter. Despite significant shifts in the DPPC:POPG isotherms, the viscosity and elasticity of the films remain relatively unaltered for all concentrations below 0.5 wt% nanoparticles. Thus, although the area at which the film reaches a given pressure is modified by the presence of the particles, the viscoelastic properties of the film are determined predominantly by the surface pressure. As noted in the previous section, there is a small increase in film elasticity at pressures above 15 mN/m amounting to a 31% increase over the phase transition region.

When the particle concentration is further increased to 0.5%, the viscosity and elasticity values are altered significantly; the film properties are not simply a function of surface pressure, shifted only in molecular area at this pressure and corresponding viscoelastic properties are achieved. Rather, the film adopts a new behaviour, likely reflecting the behaviour of a fully saturated nanoparticle film. In particular the elasticity is now impacted even at low pressures, reaching values, at the peak maximum, four times those of the other films. The earlier collapse of the film is noticeable by the distinct decrease in elasticity starting around 30 mN/m. For both viscosity and elasticity the data is significantly more scattered which may also be an indicator that the

measurements no longer reflect a lipid film but rather a nanoparticle film. In this case, the amplitude and frequency used for the measurements were optimized for lipid film measurements and the scatter may indicate a need for different parameters[104].

Similar effects are seen with Infasurf. For particle concentrations lower than 0.5 wt%, the viscosity and elasticity are determined simply by the surface pressure of the film, even if the area at which this pressure occurs is altered. Again, a high particle concentration of 0.5 wt% can induce changes to the viscosity or elasticity of the film at a given surface pressure, but the effects are much more subtle, likely due to charge screening of the anionic lipid by the cationic SP-B protein.

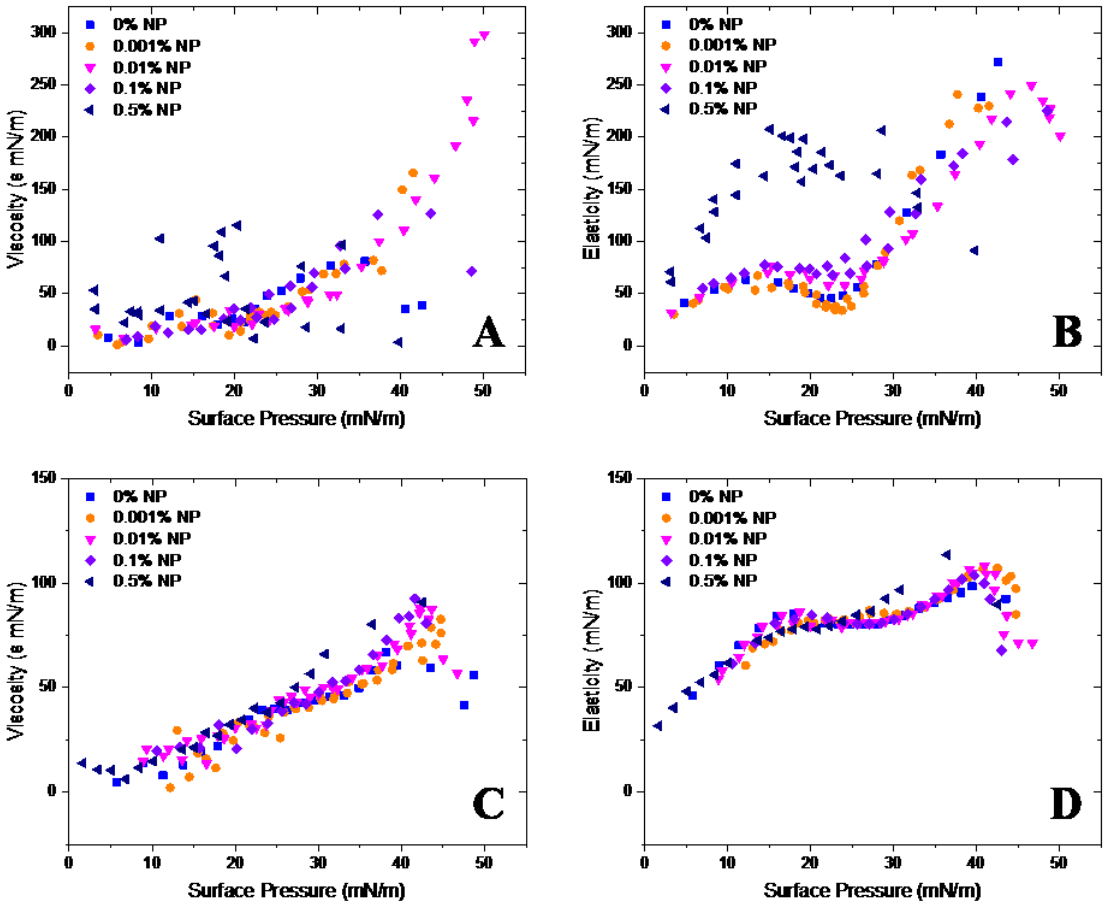

Figure 20. Viscoelasticity measurements of 70:30 DPPC:POPG (A and B) and Infasurf (C and D) monolayers in cationic nanoparticles with increasing particle concentration at room temperature.

3.3.2. Impact of anionic nanoparticles as a function of concentration

The surface pressure–area isotherms of the two monolayer systems in the presence of anionic nanoparticles at different concentrations are shown in Figure 21. For the DPPC:POPG isotherms, the phase transition is still present, however, with the anionic nanoparticles present in the subphase, it is less distinct than it was with cationic nanoparticles. As with the cationic nanoparticles there is a non-monotonic increase in molecular area with increasing concentration of anionic nanoparticles in the subphase. In principle, the monolayer is negatively charged but it is not a homogeneous film and the anionic nanoparticles may interact with the zwitterionic DPPC-rich condensed phase. Although the shifts with increasing concentration of anionic

nanoparticles exhibit the same non-monotonic trend as observed with cationic nanoparticles, the isotherm at the highest anionic nanoparticle concentration of 0.5 wt% does not show the distinct change in isotherm shape or reduction in collapse pressure observed with cationic nanoparticles. Guzman *et al*. showed a similar result with 1 wt% anionic silica nanoparticles interaction with DPPC:DOPC:Cholesterol, namely a shift to higher surface areas[104]. For DPPC:POPG there is relatively little shape change, indicating that the expansion may be a simple excluded area effect while the phosphocholine and cholesterol system exhibits subtle shape changes suggesting an additional interaction with the lipid components. The charge repulsion may reduce such effects in DPPC:POPG in agreement with the lack of change to the condensed phase structure discussed in section 3.2.3[104].

The isotherms for Infasurf in the presence of anionic nanoparticles again show smaller shifts to higher molecular areas with similar shape to the isotherm in the absence of nanoparticles or in the presence of cationic nanoparticles (Figure 21). In agreement with the DPPC:POPG results, the isotherm of Infasurf on a subphase of 0.5 wt% anionic nanoparticles does not exhibit the changes in the squeeze-out plateau observed at high concentrations of cationic nanoparticles.

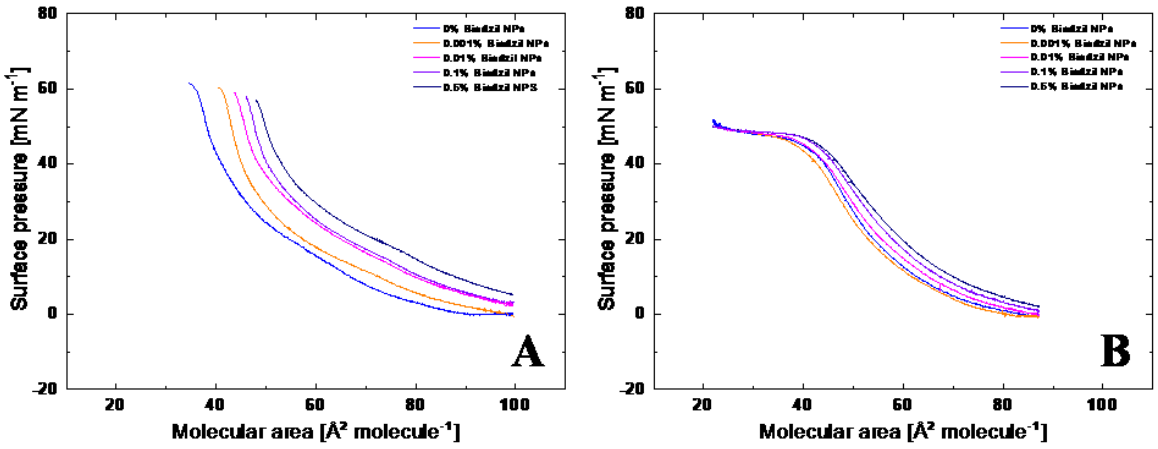

Figure 21. Surface pressure–area isotherms of 70:30 DPPC:POPG (A) and Infasurf (B) monolayers in anionic nanoparticles with increasing particle concentration at room temperature.

On the other hand, despite the isotherms appearing to exhibit only shifts to higher molecular, the viscosity and elasticity of the monolayers are distinctly altered in the presence of anionic nanoparticles (Figure 22). For the DPPC:POPG system, an effect on viscosity is seen even with the lowest nanoparticle concentration, although impact on elasticity is only observed for 0.01 wt% and higher nanoparticle concentrations. Specifically, although the shape of viscosity versus surface pressure and elasticity versus surface pressure curves have similar shapes, the increase in viscosity and elasticity associated with the loss of the LE phase appears to shift to higher molecular areas. Also, the changes associated with the LE-C phase transition are less distinct in the presence of nanoparticles. As discussed in section 3.1, at surface pressures of 30 mN/m and above, POPG begins to be squeezed-out of the monolayer and the viscosity and elasticity increase as the film begins to comprise a greater proportion of DPPC-rich condensed phase. The viscosity and elasticity data appear to be more sensitive to the proportion of the two phases than the isotherms[105]. The loss of the negatively charged LE phase appears delayed (likely due to repulsion with the anionic nanoparticles in the subphase), moreover the loss appears to occur over a narrower range of surface pressures (sharper transition). Of course, as the anionic LE phase is lost, the attraction of the anionic nanoparticles to the residual zwitterionic DPPC-rich condensed phase increases. Additionally, POPG shields the surface from being completely saturated with the anionic nanoparticles and therefore the drastic shape change at 0.5% nanoparticle concentration was not observed. It should be noticed that with increasing nanoparticle concentration it becomes more difficult to replicate data.

As with DPPC:POPG, Infasurf exhibits distinct changes in viscosity and elasticity in the presence of anionic nanoparticles, in contrast to the presence of cationic nanoparticles, despite the similarity in isotherms. The viscosity is increased subtly around 30 mN/m but it must also be noted that the data is also more scattered. On the other hand, the elasticity is significantly impacted in the presence of anionic nanoparticles. A significant increase in elasticity is observed with the lowest anionic nanoparticle concentration and this effect is observed with the higher nanoparticle concentration as well. The elasticity starts to increase at 15-20 mN/m (which is the end of the phase transition) and elasticity increases by approximately 29% compared to the absence of nanoparticles (Figure 22-D). For the 0.001% and 0.01% the elasticity values reach a maximum at 25 mN/m and then decreases to return to values similar to those in the absence of

nanoparticles. However, for the higher concentrations of nanoparticles (0.1 wt% and 0.5 wt%) the decrease in elasticity only begins at higher pressure values (37 mN/m).

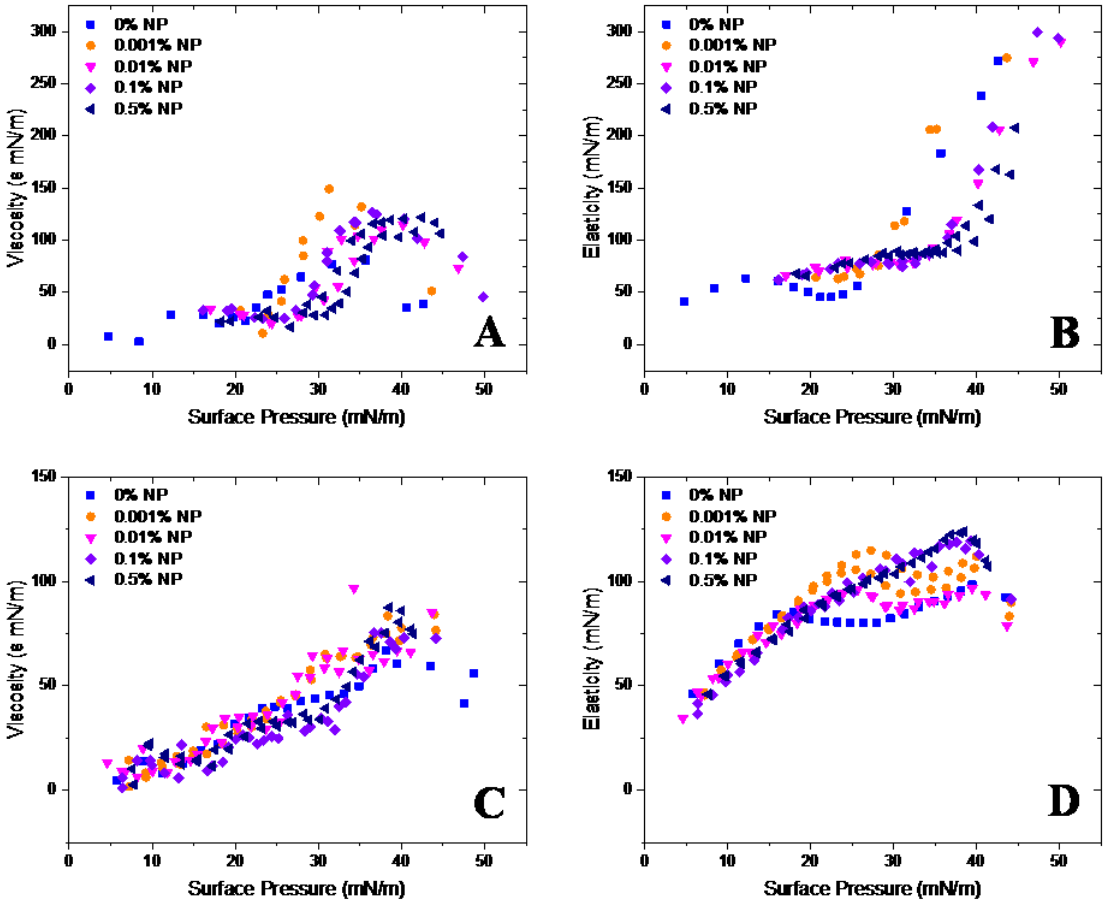

Figure 22. Viscoelasticity measurements of 70:30 DPPC:POPG (A and B) and Infasurf (C and D) monolayers in anionic nanoparticles with increasing particle concentration at room temperature.

Broicksitter *et al*. studied the effect of cationic and anionic polymer nanoparticle exposure on lung surfactant by co-spreading polylactic acid nanoparticles on Curosurf. They observed that upon the addition of nanoparticles there was a decrease in the amount of protein present. Binding of proteins to the nanoparticles caused a decrease in lung surfactant activity. This effect was more significant with the use of negatively charged nanoparticles rather than positively charged nanoparticles since SP-B and SP-C have an overall positive charge. Furthermore, this effect

occurred in a dose dependent manner where the surfactant monolayer was observed to have lost all surface activity at high concentration of anionic nanoparticles (about 0.1 wt% of nanoparticles)[106]. Similarly, with the charged silica nanoparticles, the impact on viscoelastic properties are significantly amplified with anionic nanoparticles compared to cationic nanoparticles, i.e. despite similar effects on the surface pressure-area isotherms, the cationic nanoparticles do not seem to have any impact on viscosity or elasticity until very high concentration of nanoparticles are present, whereas, the anionic nanoparticles impact the mechanical properties at even the lowest nanoparticle concentration. As mentioned before, the surface active proteins are viscosity and elasticity regulators, however, if they are bound to nanoparticles then they will not be able to carry out their functions. Although it takes a significantly larger concentration of cationic nanoparticles to see an effect on viscoelastic properties, the effect is observed and it also shows that anionic nanoparticles are indeed more potent in decreasing lung surfactant mechanical properties. This was also observed by Sachan and Galla who studied the interaction of polyorganosiloxane nanoparticles with model lung surfactant monolayer. They concluded that although SP-C protein is present in very small amount it plays a crucial role, they help anchor the collapsed unsaturated lipids during monolayer compression which can be observed as protrusions below the surface of the monolayer, in the presence of nanoparticles there was a decrease in the number and height of protrusions. Furthermore, this decrease in number of protrusions was also dose dependent, where the effect was more evident with high nanoparticle concentrations (0.1 wt%)[107]. Ramazani and Larson ran molecular simulations to study the effect of nanoparticle hydrophobicity with lipid and protein interaction. They have concluded that when the nanoparticle is hydrophobic in nature the lipid tail will interact with the nanoparticle surface and the SP-C protein will be interacting with the hydrophilic lipid headgroup. However, with decreasing hydrophobicity both lipid and protein will be in contact with the nanoparticle surface. When the nanoparticle is hydrophilic in nature then the nanoparticle will mainly be in contact with the SP-C protein on its surface and the lipids will be in contact with the protein[108].

Chapter 4. Conclusions and future work

Four different monolayers were studied as models of lung surfactant films in order to gain a better understanding of the roles of the different phases and components. Three lipid only films and one lipid-protein mixture were studied. The lipid only systems included a single component system to represent the condensed phase of lung surfactant and two binary mixtures that represent the phase separation in lung surfactant. For the latter, one comprised a zwitterionic liquid expanded phase and the other an anionic liquid expanded phase. The lipid protein mixture, that comprised a natural extract of bovine lung surfactant, is significantly more complex in composition which can hinder interpretation. The similarity in impact of nanoparticles on Infasurf and DPPC:POPG films demonstrate that the charged liquid expanded phase is a necessary component in order to better mimic the natural system. This is an important finding given that DPPC or phosphocholine mixtures are frequently used to represent lung surfactant[52,69,90,109].

We find that anionic silica nanoparticles have a greater impact on film mechanical properties but only at high pressures when charge repulsion of the particles and the charged LE phase becomes important. Guzman *et al*. also found that the impact of anionic silica was greatest at high surface pressures and led to a weakening of the monolayer cohesive forces[104]. Despite these mechanical property changes, the anionic particles had relatively little impact on condensed phase structure. On the other hand, cationic nanoparticles impact the structure of the condensed phase islands but not the rheology. There is relatively little literature to date on the impact of hydrophilic cationic nanoparticles. Taken together these results suggest that the LE-C balance is more important in determining viscosity and elasticity than the structure within the condensed phase islands, however the structure may have other relevance for stability of the phase at high pressure for example. Moreover, it appears that the anionic nanoparticles impact the macroscale properties of the films while the cationic particles impact more the molecular scale properties.

To better understand the biophysical consequences of the isotherm and rheological changes, the impact on effective surface pressure and rheology for the same molecular area range must be compared. As an example, in the absence of nanoparticles the DPPC:POPG film can cycle between a molecular area of 80-40 $Å^2$/molecule which corresponds to a surface pressure range of 0-60 mN/m. However, in the presence of 0.5% nanoparticles at an area of 80 $Å^2$/ molecule the

lipid film is already at 10 mN/m, which corresponds to the LE-C phase transition, and it collapses at 50 mN/m before it can even reach 40 $Å^2$/molecule (refer to Figure 20-B). This would mean in the presence of nanoparticles the lung surfactant will be unable to reach the very high surface pressure values that it can normally reach and will collapse at a lower surface pressure. The lung has a fixed area range and this will alter minimum the maximum surface pressures the lung can reach during the breathing cycle and cause a premature film collapse.

While much of the literature has focused on relatively high nanoparticle concentrations (1 wt%), we have shown that structural and rheological changes can be observed at concentrations as low as 0.001 wt%, i.e. 1000 times lower than previously reported. Moreover, at the higher concentrations, the membrane properties take on characteristics of a particle-laden film which may not be realistic for airborne pollutants. This work highlights the potential detrimental impact of airborne nanoparticles on lung surfactant functioning at low concentrations.

One drawback of the methodology is that it uses adsorption from the subphase as the mechanism of particle-film interactions. In order to make the deposition more realistic, future studies should focus on introducing the nanoparticles from the air-side to better mimic nanoparticle inhalation. For these studies, the frequency of oscillation was optimized for the lipid films. It was held constant throughout the experiments in order to make comparisons since the absolute values of elasticity and viscosity vary with the frequency and amplitude[83]. However, as the amount of nanoparticles at the interface increases, the optimal frequency for measurement may need to be modified. This plays a particularly important role at high nanoparticle concentrations.

Finally, while the DPPC:POPG presented the best mimetic of Infasurf, it is still only a binary mixture and lacks certain relevant components. Specifically, Infasurf is known to contain cholesterol which can induce a liquid-ordered phase and is a known membrane fluidity buffer[73]. A ternary system comprising DPPC:POPG:Cholesterol would provide a useful intermediate for understanding the behavior of Infasurf and may be a better simplified lipid only model. Additionally, SP-B and SP-C can be purified[4,56,72] and these could be systematically added to the lipid systems to better understand the role of the proteins.

References

1. Finlayson-Pitts, B. J. (1997). Tropospheric Air Pollution: Ozone, Airborne Toxics, Polycyclic Aromatic Hydrocarbons, and Particles. *Science*, 276(5315), 1045-1051.
2. Basha, M. A., Gross, K. B., Gwizdala, C. J., Haidar, A. H., & Popovich, J. (1994). Bronchoalveolar Lavage Neutrophilia in Asthmatic and Healthy Volunteers After Controlled Exposure to Ozone and Filtered Purified Air. *Chest*, 106(6), 1757-1765.
3. Ge, M. Q., Kokalari, B., Flayer, C. H., Killingbeck, S. S., Redai, I. G., Macfarlane, A. W., Haczku, A. (2016). Cutting Edge: Role of NK Cells and Surfactant Protein D in Dendritic Cell Lymph Node Homing: Effects of Ozone Exposure. *The Journal of Immunology*, 196(7), 3212-3212.
4. Hemming, J. M., Hughes, B. R., Rennie, A. R., Tomas, S., Campbell, R. A., Hughes, A. V., Thompson, K. C. (2015). Environmental Pollutant Ozone Causes Damage to Lung Surfactant Protein B (SP-B). *Biochemistry*, 54(33), 5185-5197.
5. Thompson, K. C., Jones, S. H., Rennie, A. R., King, M. D., Ward, A. D., Hughes, B. R., Hughes, A. V. (2013). Degradation and Rearrangement of a Lung Surfactant Lipid at the Air–Water Interface during Exposure to the Pollutant Gas Ozone. *Langmuir*, 29(14), 4594-4602.
6. Chan-Yeung, M.; Dimich-Ward, H. (2003). Respiratory Health Effects of Exposure to Environmental Tobacco Smoke. *Respirology*, 8, 131–139.
7. Ning, Z., Cheung, C., Fu, J., Liu, M., & Schnell, M. (2006). Experimental study of environmental tobacco smoke particles under actual indoor environment. *Science of The Total Environment*, 367(2-3), 822-830.
8. Larsson, M. L.; Frisk, M.; Hallstrom, J.; Kiviloog, J.; Lundback, B. (2001). Environmental Tobacco Smoke Exposure during Childhood Is Associated with Increased Prevalence of Asthma in Adults. *Chest*, 120, 711–717.
9. Johnson, K. C., Hu, J., Mao, Y., Paulse, B., Dewar, R., Dryer, D., & Fincham, S. (2001). Lifetime residential and workplace exposure to environmental tobacco smoke and lung cancer in never-smoking women, Canada 1994-97. *International Journal of Cancer*, 93(6), 902-906.

10. Bringezu, F., Pinkerton, K. E., & Zasadzinski, J. A. (2003). Environmental Tobacco Smoke Effects on the Primary Lipids of Lung Surfactant. *Langmuir*, 19(7), 2900-2907.
11. Subramaniam, S., Bummer, P., & Gairola, C. G. (1995). Biochemical and Biophysical Characterization of Pulmonary Surfactant in Rats Exposed Chronically to Cigarette Smoke. *Fundamental and Applied Toxicology*, 27(1), 63-69.
12. Taylor, D. A. (2002). Dust in the Wind. Environmental Health Perspectives, 110, 80-87.
13. Shi, Z.; Shao, L.; Jones, T. P.; Lu, S. (2005). Microscopy and Mineralogy of Airborne Particles Collected during Severe Dust Storm Episodes in Beijing, China. *Journal of Geophysical Research*, 110.
14. Husar, R. B.; Tratt, D. M.; Schichtel, B. A.; Falke, S. R.; Li, F.; Jaffe, D.; Gasso, S.; Gill, T.; Laulainen, N. S.; Lu, F.; *et al*. (2001). Asian Dust Events of April 1998. *Journal of Geophysical Research,* 106, 18317–18330.
15. Sapkota, A.; Symons, J. M.; Kleissl, J.; Wang, L.; Parlange, M. B.; Ondov, J.; Breysse, P. N.; Diette, G. B.; Eggleston, P. A.; Buckley, T. J. (2005). Impact of the 2002 Canadian Forest Fires on Particulate Matter Air Quality in Baltimore City. *Environmental Science & Technology*, 39, 24–32.
16. Mott, J. A.; Meyer, P.; Mannino, D.; Redd, S. C.; Smith, E. M.; Gotway-Crawford, C.; Chase, E. (2002). Wildland Forest Fire Smoke: Health Effects and Intervention Evaluation, Hoopa, California, 1999. *Western Journal of Medicine*, 176, 157–162.
17. Blundell, G.; Henderson, W. J.; Price, E. W. (1989). Soil Particles in the Tissues of the Foot in Endemic Elephantiasis of the Lower Legs. *Annals of Tropical Medicine & Parasitology*, 83, 381–385.
18. Corachan, M.; Tura, J. M.; Campo, E.; Soley, M.; Traveria, A. (1988). Podoconiosis in Aequatorial Guinea. Report of Two Cases from Different Geological Environments. *Tropical and Geographical Medicine*, 40, 359–364.
19. Ris, C. U.S. (2007). EPA Health Assessment for Diesel Engine Exhaust: A Review. *Inhalation Toxicology*, 19, 229–239.
20. Westerdahl, D.; Fruin, S.; Sax, T.; Fine, P. M.; Sioutas, C. (2005). Mobile Platform Measurements of Ultrafine Particles and Associated Pollutant Concentrations on Freeways and Residential Streets in Los Angeles. *Atmospheric Environment*, 39, 3597–3610.

21. Stefani, D.; Wardman, D.; Lambert, T. (2005). The Implosion of the Calgary General Hospital: Ambient Air Quality Issues. *Journal of the Air & Waste Management Association*, 55, 52–59.
22. Sioutas, C.; Delfino, R. J.; Singh, M. (2005). Exposure Assessment for Atmospheric Ultrafine Particles (UFPs) and Implications in Epidemiologic Research. *Environmental Health Perspectives*, 113, 947–955.
23. Afshari, A.; Matson, U.; Ekberg, L. E. (2005). Characterization of Indoor Sources of Fine and Ultrafine Particles: A Study Conducted in a Full-Scale Chamber. *Indoor Air*, 15, 141–150.
24. See, S. W.; Balasubramanian, R. (2006). Risk Assessment of Exposure to Indoor Aerosols Associated with Chinese Cooking. *Environmental Research*, 102, 197–204.
25. Vermylen, J.; Nemmar, A.; Nemery, B.; Hoylaerts, M. F. (2005). Ambient Air Pollution and Acute Myocardial Infarction. *Journal of Thrombosis and Haemostasis*, 3, 1955–1961.
26. Hoek, G.; Brunekreef, B.; Goldbohm, S.; Fischer, P.; van, den B. P. A. (2002). Association between Mortality and Indicators of Traffic-Related Air Pollution in the Netherlands: A Cohort Study. *The Lancet*, 360, 1203–1209.
27. Garshick, E.; Schenker, M. B.; Munoz, A.; Segal, M.; Smith, T. J.; Woskie, S. R.; Hammond, S. K.; Speizer, F. E. (1988). A Retrospective Cohort Study of Lung Cancer and Diesel Exhaust Exposure in Railroad Workers. *The American Review of Respiratory Disease*, 137, 820–825.
28. Rushton, L. (2004). Health Impact of Environmental Tobacco Smoke in the Home. *Reviews on Environmental Health*, 19, 291–309.
29. Husgafvel-Pursiainen, K. (2004). Genotoxicity of Environmental Tobacco Smoke: A Review. *Mutation Research, Reviews in Mutation Research*, 567, 427–445.
30. Shrivas, K.; Shankar, R.; Dewangan, K. (2015). Gold Nanoparticles as a Localized Surface Plasmon Resonance Based Chemical Sensor for on-Site Colorimetric Detection of Arsenic in Water Samples. *Sensors and Actuators B*, 220, 1376–1383.
31. Yang, D., Wang, T., Su, Z., Xue, L., Mo, R., & Zhang, C. (2016). Reversing Cancer Multidrug Resistance in Xenograft Models via Orchestrating Multiple Actions of

Functional Mesoporous Silica Nanoparticles. *ACS Applied Materials & Interfaces*, *8*(34), 22431-22441.

32. Wang, S. High-Strength Anti-Aging Computer Cable., July 13, 2016.
33. Yu, J. X., & Li, T. H. (2011). Distinct biological effects of different nanoparticles commonly used in cosmetics and medicine coatings. *Cell & Bioscience*, *1*(1), 19.
34. Mo, Z. Toothpaste Containing Zinc Oxide Nanoparticles for Preventing Gingivitis and Periodontitis., April 29, 2015.
35. Maier, L. A. (2002). Clinical Approach to Chronic Beryllium Disease and Other Nonpneumoconiotic Interstitial Lung Diseases. *Journal of Thoracic Imaging*, 17, 273–284.
36. Paris, C.; Bertrand, O.; de, A. R. R. (2004). Lung Cancer and Occupational Exposures (asbestos Not Considered). *La Revue du Praticien*, 54, 1660–1664.
37. Waalkes, M. P. (2003). Cadmium Carcinogenesis. *Mutation Research, Fundamental and Molecular Mechanisms of Mutagenesis*, 533, 107–120.
38. Mannino, D. M.; Holguin, F.; Greves, H. M.; Savage-Brown, A.; Stock, A. L.; Jones, R. L. (2004). Urinary Cadmium Levels Predict Lower Lung Function in Current and Former Smokers: Data from the Third National Health and Nutrition Examination Survey. *Thorax*, 59, 194–198.
39. McGrath, K. G. (2003). An Earlier Age of Breast Cancer Diagnosis Related to More Frequent Use of Antiperspirants/deodorants and Underarm Shaving. *European Journal of Cancer Prevention*, 12, 479–485.
40. Guillard, O.; Fauconneau, B.; Olichon, D.; Dedieu, G.; Deloncle, R. (2004). Hyperaluminemia in a Woman Using an Aluminum-Containing Antiperspirant for 4 Years. *American Journal of Medicine*, 117, 956–959.
41. Kawahara, M. (2005). Effects of Aluminum on the Nervous System and Its Possible Link with Neurodegenerative Diseases. *Journal of Alzheimer's Disease*, 8, 171–182; discussion 209–215.
42. Miu, A. C.; Benga, O. (2006). Aluminum and Alzheimer's Disease: A New Look. *Journal of Alzheimer's Disease*, 10, 179–201.

43. Antonini, J. M.; Santamaria, A. B.; Jenkins, N. T.; Albini, E.; Lucchini, R. (2006). Fate of Manganese Associated with the Inhalation of Welding Fumes: Potential Neurological Effects. *NeuroToxicology*, 27, 304–310.
44. Weiss, B. (2006). Economic Implications of Manganese Neurotoxicity. *NeuroToxicology*, 27, 362–368.
45. Noonan, C. W.; Pfau, J. C.; Larson, T. C.; Spence, M. R. (2006). Nested Case-Control Study of Autoimmune Disease in an Asbestos-Exposed Population. *Environmental Health Perspectives*, 114, 1243–1247.
46. Markovits, D.; Schapira, D.; Wiener, A.; Nahir, A. M. (2003). Silica-Related Rheumatoid Arthritis without Lung Involvement. *Clinical Rheumatology*, 22, 53–55.
47. Schurch, S.; Goerke, J.; Clements, J. A. (1976). Direct Determination of Surface Tension in the Lung. *Proceedings of the National Academy of Sciences of the United States of America*, 73, 4698–4702.
48. Alonso, C.; Alig, T.; Yoon, J.; Bringezu, F.; Warriner, H.; Zasadzinski, J. A. (2004). More than a Monolayer: Relating Lung Surfactant Structure and Mechanics to Composition. *Biophysical Journal*, 87, 4188–4202.
49. Bernardino, de la S. J.; Perez-Gil, J.; Simonsen, A. C.; Bagatolli, L. A. (2004). Cholesterol Rules: Direct Observation of the Coexistence of Two Fluid Phases in Native Pulmonary Surfactant Membranes at Physiological Temperatures. *The Journal of Biological Chemistry*, 279, 40715–40722.
50. Zasadzinski, J. A.; Ding, J.; Warriner, H. E.; Bringezu, F.; Waring, A. J. (2001). The Physics and Physiology of Lung Surfactants. *Current Opinion in Colloid & Interface Science*, 6, 506–513.
51. Alonso, C.; Bringezu, F.; Brezesinski, G.; Waring, A. J.; Zasadzinski, J. A. (2005). Modifying Calf Lung Surfactant by Hexadecanol. *Langmuir*, 21, 1028–1035.
52. Ding, J.; Takamoto, D. Y.; Von Nahmen, A.; Lipp, M. M.; Lee, K. Y. C.; Waring, A. J.; Zasadzinski, J. A. (2001). Effects of Lung Surfactant Proteins, SP-B and SP-C, and Palmitic Acid on Monolayer Stability. *Biophysical Journal*, 80, 2262–2272.
53. Hawgood, S. (2004). Surfactant Protein B: Structure and Function. *Biology of the Neonate*, 85, 285–289.

54. Notter, R. H.; Wang, Z.; Egan, E. A.; Holm, B. A. (2002). Component-Specific Surface and Physiological Activity in Bovine-Derived Lung Surfactants. *Chemistry and Physics of Lipids*, 114, 21–34.
55. Sharifahmadian, M.; Sarker, M.; Palleboina, D.; Waring, A. J.; Walther, F. J.; Morrow, M. R.; Booth, V. (2013). Role of the N-Terminal Seven Residues of Surfactant Protein B (SP-B). *PLoS One*, 8.
56. Bringezu, F.; Ding, J.; Brezesinski, G.; Waring, A. J.; Zasadzinski, J. A. (2002). Influence of Pulmonary Surfactant Protein B on Model Lung Surfactant Monolayers. *Langmuir*, 18, 2319–2325.
57. Veldhuizen, E. J., & Haagsman, H. P. (2000). Role of pulmonary surfactant components in surface film formation and dynamics. *Biochimica et Biophysica Acta (BBA) - Biomembranes*, *1467*(2), 255-270.
58. LeVine, A. M., Whitsett, J. A., Gwozdz, J. A., Richardson, T. R., Fisher, J. H., Burhans, M. S., & Korfhagen, T. R. (2000). Distinct Effects of Surfactant Protein A or D Deficiency During Bacterial Infection on the Lung. *The Journal of Immunology*, *165*(7), 3934-3940.
59. Korfhagen, T. R., Sheftelyevich, V., Burhans, M. S., Bruno, M. D., Ross, G. F., Wert, S. E., … Fisher, J. H. (1998). Surfactant Protein-D Regulates Surfactant Phospholipid Homeostasisin Vivo. *Journal of Biological Chemistry*, *273*(43), 28438-28443.
60. Cockshutt, A. M.; Weitz, J.; Possmayer, F. (1990). Pulmonary Surfactant-Associated Protein A Enhances the Surface Activity of Lipid Extract Surfactant and Reverses Inhibition by Blood Proteins in Vitro. *Biochemistry*, 29, 8424–8429.
61. Kishore, U.; Greenhough, T. J.; Waters, P.; Shrive, A. K.; Ghai, R.; Kamran, M. F.; Lopez Bernal, A.; Reid, K. B. M.; Madan, T.; Chakraborty, T. (2006). Surfactant Proteins SP-A and SP-D: Structure, Function and Receptors. *Molecular Immunology*, 43, 1293–1315.
62. Hartshorn, K. L.; Crouch, E. C.; White, M. R.; Eggleton, P.; Tauber, A. I.; Chang, D.; Sastry, K. (1994). Evidence for a Protective Role of Pulmonary Surfactant Protein D (SP-D) against Influenza A Viruses. *Journal of Clinical Investigation*, 94, 311–319.

63. Kishore, U.; Madan, T.; Sarma, P. U.; Singh, M.; Urban, B. C.; Reid, K. B. M. (2002). Protective Roles of Pulmonary Surfactant Proteins, SP-A and SP-D, against Lung Allergy and Infection Caused by Aspergillus Fumigatus. *Immunobiology*, 205, 610–618.
64. Alonso, C.; Waring, A.; Zasadzinski, J. A. (2005). Keeping Lung Surfactant Where It Belongs: Protein Regulation of Two-Dimensional Viscosity. *Biophysical Journal*, 89, 266–273.
65. Johansson, J. (1998). Structure and Properties of Surfactant Protein C. *Biochimica et Biophysica Acta, Molecular Basis of Disease*, 1408, 161–172.
66. Schurch, S.; Green, F. H. Y.; Bachofen, H. (1998). Formation and Structure of Surface Films: Captive Bubble Surfactometry. *Biochimica et Biophysica Acta, Molecular Basis of Disease*, 1408, 180–202.
67. Perez-Gil, J.; Weaver, T. E. (2010). Pulmonary Surfactant Pathophysiology: Current Models and Open Questions. *Physiology*, 25, 132–141.
68. Bringezu, F., Ding, J., Brezesinski, G., Zasadzinski, J. A. (2001). Changes in Model Lung Surfactant Monolayers Induced by Palmitic Acid. *Langmuir*, *17*(15), 4641-4648.
69. Guzman, E.; Liggieri, L.; Santini, E.; Ferrari, M.; Ravera, F. (2012). DPPC-DOPC Langmuir Monolayers Modified by Hydrophilic Silica Nanoparticles: Phase Behaviour, Structure and Rheology. *Colloids and Surfaces*, 413, 174–183.
70. Anton, N.; Saulnier, P.; Boury, F.; Foussard, F.; Benoit, J.-P.; Proust, J. E. (2007). The Influence of Headgroup Structure and Fatty Acyl Chain Saturation of Phospholipids on Monolayer Behavior: A Comparative Rheological Study. *Chemistry and Physics of Lipids*, 150, 167–175.
71. Rodriguez-Capote, K., Nag, K., Schürch, S., & Possmayer, F. (2001). Surfactant protein interactions with neutral and acidic phospholipid films. *American Journal of Physiology-Lung Cellular and Molecular Physiology*, *281*(1), L231-L242.
72. Bakshi, M. S., Zhao, L., Smith, R., Possmayer, F., & Petersen, N. O. (2008). Metal Nanoparticle Pollutants Interfere with Pulmonary Surfactant Function In Vitro. *Biophysical Journal*, *94*(3), 855-868.
73. Zhang, H.; Fan, Q.; Wang, Y. E.; Neal, C. R.; Zuo, Y. Y. (2011). Comparative Study of Clinical Pulmonary Surfactants Using Atomic Force Microscopy. *Biochimica et Biophysica Acta, Biomembranes*, 1808, 1832–1842.

74. Dizdar, E. A.; Sari, F. N.; Aydemir, C.; Oguz, S. S.; Erdeve, O.; Uras, N.; Dilmen, U. (2012). A Randomized, Controlled Trial of Poractant Alfa versus Beractant in the Treatment of Preterm Infants with Respiratory Distress Syndrome. *American Journal of Perinatology*, 29, 95–100.
75. Zhang, L.; Cao, H.-Y.; Zhao, S.; Yuan, L.-J.; Han, D.; Jiang, H.; Wu, S.; Wu, H.-M. (2015). Effect of Exogenous Pulmonary Surfactants on Mortality Rate in Neonatal Respiratory Distress Syndrome: A Network Meta-Analysis of Randomized Controlled Trials. *Pulmonary Pharmacology and Therapeutics*, 34, 46–54.
76. Bloom, B. T.; Kattwinkel, J.; Hall, R. T.; Delmore, P. M.; Egan, E. A.; Trout, J. R.; Malloy, M. H.; Brown, D. R.; Holzman, I. R.; Coghill, C. H.; *et al*. (1997). Comparison of Infasurf (calf Lung Surfactant Extract) to Survanta (Beractant) in the Treatment and Prevention of Respiratory Distress Syndrome. *Pediatrics*, 100, 31–38.
77. Zhang, H., Wang, Y. E., Fan, Q., & Zuo, Y. Y. (2011). On the Low Surface Tension of Lung Surfactant. *Langmuir*, *27*(13), 8351-8358.
78. Lin, X.; Zuo, Y. Y.; Gu, N. (2015). Shape Affects the Interactions of Nanoparticles with Pulmonary Surfactant. *Science China Materials*, 58, 28–37.
79. Harishchandra, R. K.; Saleem, M.; Galla, H.-J. (2010). Nanoparticle Interaction with Model Lung Surfactant Monolayers. *Journal of The Royal Society Interface*, 7.
80. Guzman, E.; Santini, E.; Ferrari, M.; Liggieri, L.; Ravera, F. (2015). Interfacial Properties of Mixed DPPC-Hydrophobic Fumed Silica Nanoparticle Layers. *The Journal of Physical Chemistry C*, 119, 21024–21034.
81. Guzman, E., Liggieri, L., Santini, E., Ferrari, M., & Ravera, F. (2012). Influence of silica nanoparticles on phase behavior and structural properties of DPPC—Palmitic acid Langmuir monolayers. *Colloids and Surfaces A: Physicochemical and Engineering Aspects*, *413*, 280-287.
82. Loglio, G.; Pandolfini, P.; Miller, R.; Makievski, A. V.; Ravera, F.; Ferrari, M.; Liggieri, L. (2001). Drop and Bubble Shape Analysis as a Tool for Dilational Rheological Studies of Interfacial Layers. *Studies in Interface Science*, 11, 439–483.
83. Wüstneck, R.; Perez-Gil, J.; Wüstneck, N.; Cruz, A.; Fainerman, V. B.; Pison, U. (2005). Interfacial Properties of Pulmonary Surfactant Layers. *Advances in Colloid and Interface Science*, 117, 33–58.

84. Vranceanu, M.; Winkler, K.; Nirschl, H.; Leneweit, G. (2008). Surface Rheology and Phase Transitions of Monolayers of Phospholipid/cholesterol Mixtures. *Biophysical Journal*, 94, 3924–3934.
85. Vranceanu, M.; Winkler, K.; Nirschl, H.; Leneweit, G. (2007). Surface Rheology of Monolayers of Phospholipids and Cholesterol Measured with Axisymmetric Drop Shape Analysis. *Colloids and Surfaces A: Physicochemical and Engineering Aspects*, 311, 140–153.
86. Krägel, J.; Kretzschmar, G.; Li, J. B.; Loglio, G.; Miller, R.; Möhwald, H. (1996). Surface Rheology of Monolayers. *Thin Solid Films*, 284, 361–364.
87. Orbulescu, J.; Mullins, O. C.; Leblanc, R. M. (2010). Surface Chemistry and Spectroscopy of UG8 Asphaltene Langmuir Film, Part 1. *Langmuir*, 26, 15257–15264.
88. Kjaer, K. (1994). Some simple ideas on X-ray reflection and grazing-incidence diffraction from thin surfactant films. *Physica B: Condensed Matter*, *198*(1-3), 100-109.
89. O'Flaherty, S. M., Wiegart, L., Konovalov, O., & Struth, B. (2005). Observation of Zinc Phthalocyanine Aggregates on a Water Surface Using Grazing Incidence X-ray Scattering. *Langmuir*, 21(24), 11161-11166.
90. Mangiarotti, A., Caruso, B., & Wilke, N. (2014). Phase coexistence in films composed of DLPC and DPPC: A comparison between different model membrane systems. *Biochimica et Biophysica Acta (BBA) - Biomembranes*, *1838*(7), 1823-1831.
91. Yun, H. J. (2003). Physicochemical Properties of Phosphatidylcholine (PC) Monolayers with Different Alkyl Chains, at the Air/Water Interface. *Bulletin of the Korean Chemical Society*, *24*(3), 377-383.
92. McConlogue, C. W., & Vanderlick, T. K. (1997). A Close Look at Domain Formation in DPPC Monolayers. *Langmuir*, *13*(26), 7158-7164.
93. Silvius, J. R. (1982). Thermotropic phase transitions of pure lipids in model membranes and their modification by membrane proteins. *Lipid-Protein Interactions*, *2*, 239-281.
94. Pimthon, J., Willumeit, R., Lendlein, A., & Hofmann, D. (2009). All-atom molecular dynamics simulation studies of fully hydrated gel phase DPPG and DPPE bilayers. *Journal of Molecular Structure*, *921*(1-3), 38-50.

95. Nojima, Y., & Iwata, K. (2014). Viscosity Heterogeneity inside Lipid Bilayers of Single-Component Phosphatidylcholine Liposomes Observed with Picosecond Time-Resolved Fluorescence Spectroscopy. *The Journal of Physical Chemistry B*, *118*(29), 8631-8641.
96. Selladurai, S. L., Miclette Lamarche, R., Schmidt, R., & DeWolf, C. E. (2016). Model Lung Surfactant Films: Why Composition Matters. *Langmuir*, *32*(41), 10767-10775.
97. McConnell, H. (1991). Structures And Transitions In Lipid Monolayers At The Air-Water Interface. *Annual Review of Physical Chemistry*, *42*(1), 171-195.
98. Chakraborty, A., Mucci, N. J., Tan, M. L., Steckley, A., Zhang, T., Forrest, M. L., & Dhar, P. (2015). Phospholipid Composition Modulates Carbon Nanodiamond-Induced Alterations in Phospholipid Domain Formation. *Langmuir*, *31*(18), 5093-5104.
99. Brezesinski, G., Dietrich, A., Struth, B., Böhm, C., Bouwman, W. G., Kjaer, K., & Möhwald, H. (1995). Influence of ether linkages on the structure of double-chain phospholipid monolayers. *Chemistry and Physics of Lipids*, *76*(2), 145-157.
100. Scherer, P. G., & Seelig, J. (1989). Electric charge effects on phospholipid headgroups. Phosphatidylcholine in mixtures with cationic and anionic amphiphiles. *Biochemistry*, *28*(19), 7720-7728.
101. Saiz, L., & Klein, M. L. (2002). Electrostatic interactions in a neutral model phospholipid bilayer by molecular dynamics simulations. *The Journal of Chemical Physics*, *116*(7), 3052-3057.
102. Sanchez, J., & Badia, A. (2008). Spatial variation in the molecular tilt orientational order within the solid domains of phase-separated, mixed dialkylphosphatidylcholine monolayers. *Chemistry and Physics of Lipids*, *152*(1), 24-37.
103. Christoforou, M., Leontidis, E., & Brezesinski, G. (2012). Effects of Sodium Salts of Lyotropic Anions on Low-Temperature, Ordered Lipid Monolayers. *The Journal of Physical Chemistry B*, *116*(50), 14602-14612.
104. Guzman, E., Ferrari, M., Santini, E., Liggieri, L., & Ravera, F. (2015). Effect of silica nanoparticles on the interfacial properties of a canonical lipid mixture. *Colloids and Surfaces B: Biointerfaces*, *136*, 971-980.
105. Alonso, C., & Zasadzinski, J. A. (2006). A Brief Review of the Relationships between Monolayer Viscosity, Phase Behavior, Surface Pressure, and Temperature Using

a Simple Monolayer Viscometer†. *The Journal of Physical Chemistry B*, *110*(44), 22185-22191.

106. Beck-Broichsitter, M. (2016). Biophysical Activity of Impaired Lung Surfactant upon Exposure to Polymer Nanoparticles. *Langmuir*, *32*(40), 10422-10429.

107. Sachan, A. K., Harishchandra, R. K., Bantz, C., Maskos, M., Reichelt, R., & Galla, H. (2012). High-Resolution Investigation of Nanoparticle Interaction with a Model Pulmonary Surfactant Monolayer. *ACS Nano*, *6*(2), 1677-1687.

108. Ramazani, A., Mandal, T., & Larson, R. G. (2016). Modeling the Hydrophobicity of Nanoparticles and Their Interaction with Lipids and Proteins. *Langmuir*, *32*(49), 13084-13094.

109. Clop, E. M., Corvalán, N. A., & Perillo, M. A. (2016). Langmuir films of dipalmitoyl phosphatidylethanolamine grafted poly(ethylene glycol). In-situ evidence of surface aggregation at the air-water interface. *Colloids and Surfaces B: Biointerfaces*, *148*, 640-649.

Appendix

Appendix A: Isotherms and Rheology Data for Bindzil DI (Neutral Particles)

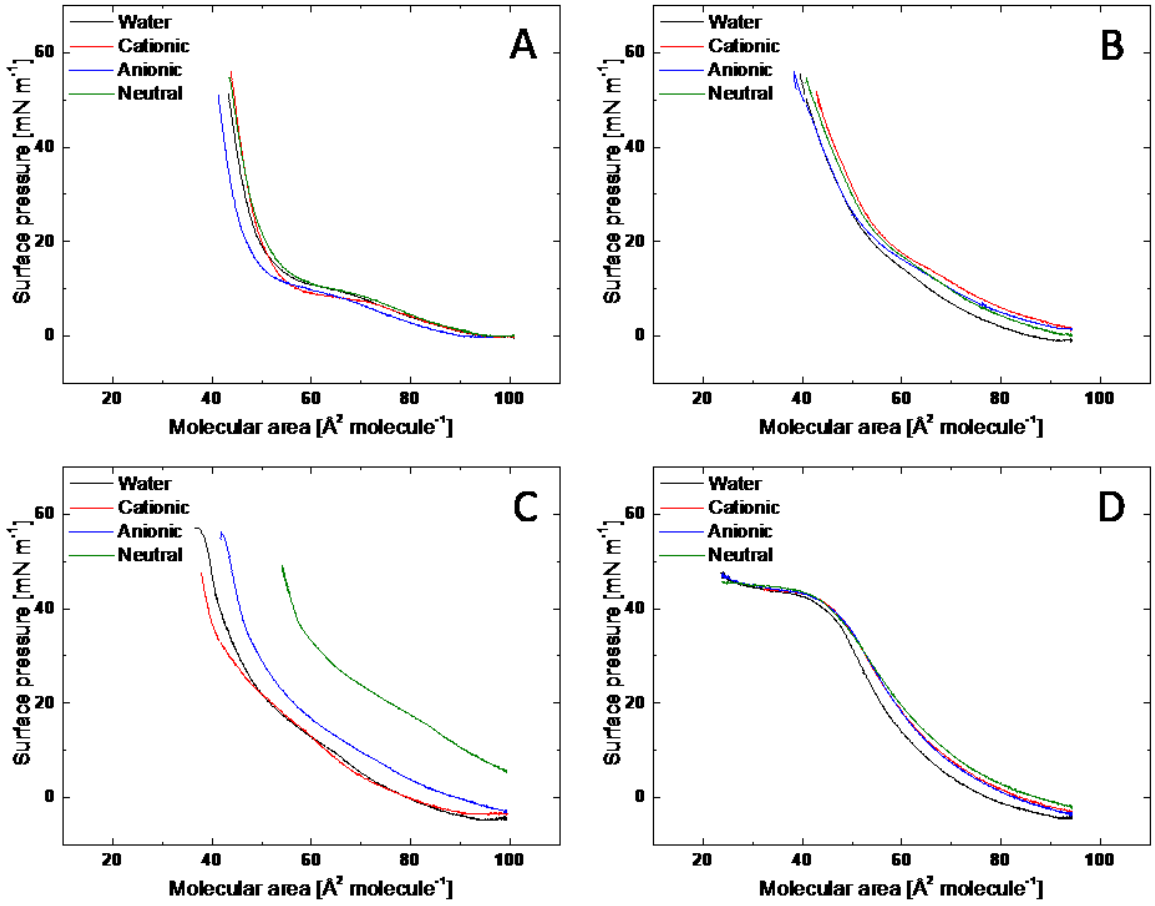

Isotherms of each of the model membrane systems (A: DPPC, B: DPPC:DLPC, C: DPPC:POPG and D: Infasurf) on the four subphases (water: black, 0.001 wt% cationic silica nanoparticles: red, 0.001 wt% anionic silica nanoparticles: blue and 0.001 wt% neutral silica nanoparticles: green).

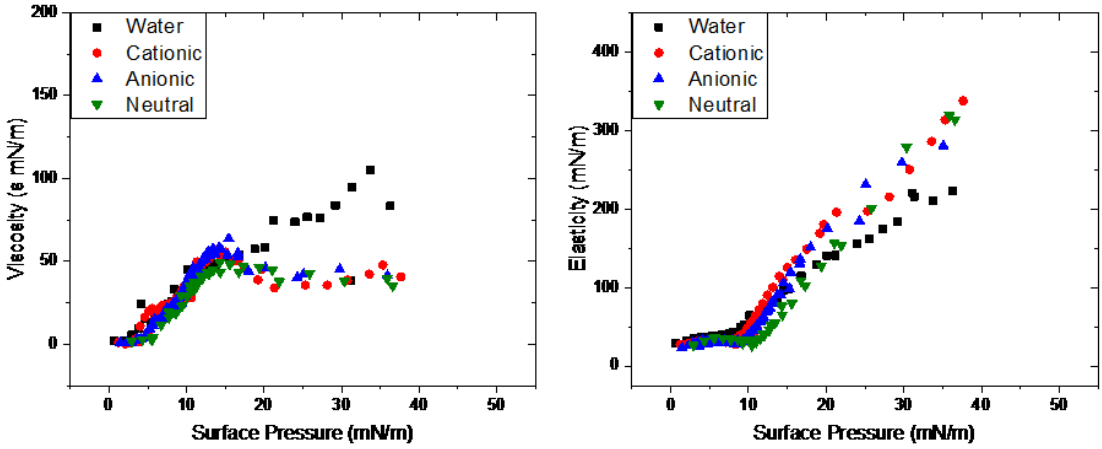

Viscoelasticity measurements of DPPC monolayers spread on different subphases at room temperature: water (black), 0.001 wt% cationic silica nanoparticles (red), 0.001 wt% anionic silica nanoparticles (blue) and 0.001 wt% neutral silica nanoparticles (green). Each data set comprises duplicate measurements made on two, independently prepared films.

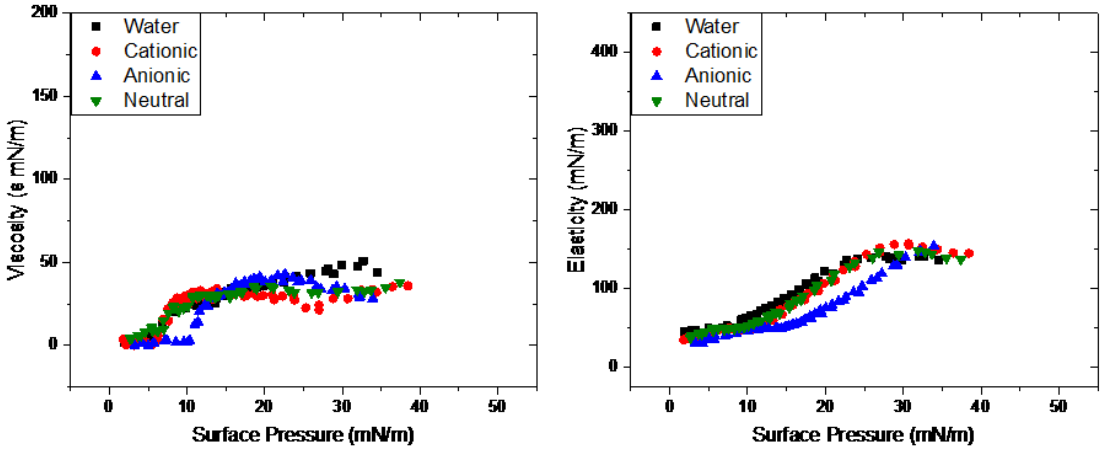

Viscoelasticity measurements of 70:30 DPPC:DLPC monolayers spread on different subphases at room temperature: water (black), 0.001 wt% cationic silica nanoparticles (red), 0.001 wt% anionic silica nanoparticles (blue) and 0.001 wt% neutral silica nanoparticles (green). Each data set comprises duplicate measurements made on two, independently prepared films.

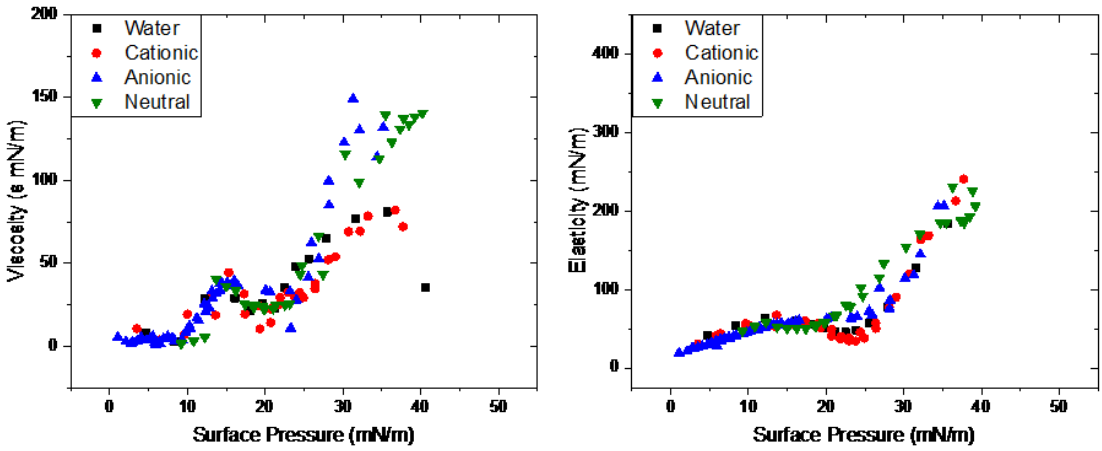

Viscoelasticity measurements of 70:30 DPPC:POPG monolayers spread on different subphases at room temperature: water (black), 0.001 wt% cationic silica nanoparticles (red), 0.001 wt% anionic silica nanoparticles (blue) and 0.001 wt% neutral silica nanoparticles (green). Each data set comprises duplicate measurements made on two, independently prepared films.

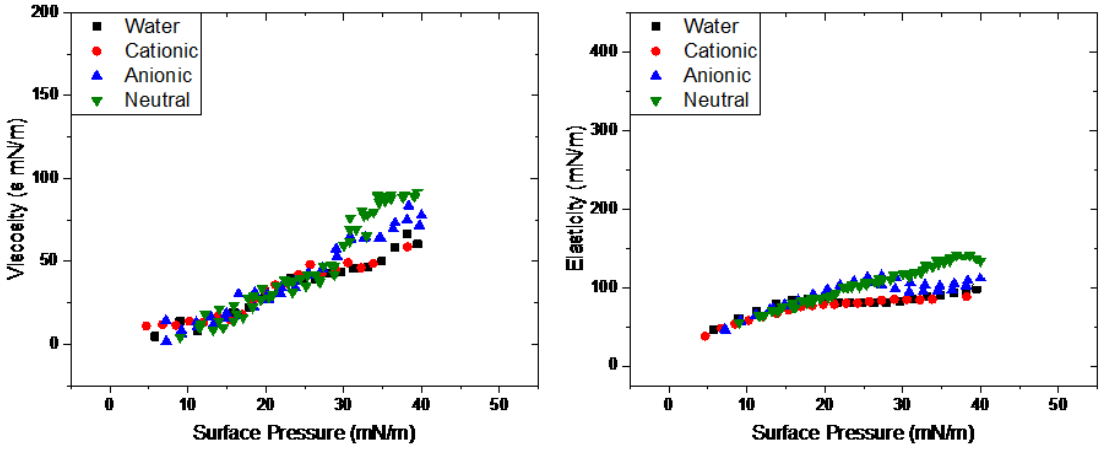

Viscoelasticity measurements of Infasurf monolayers spread on different subphases at room temperature: water (black), 0.001 wt% cationic silica nanoparticles (red), 0.001 wt% anionic silica nanoparticles (blue) and 0.001 wt% neutral silica nanoparticles (green). Each data set comprises duplicate measurements made on two, independently prepared films.

Appendix B: GIXD Data for Infasurf monolayers

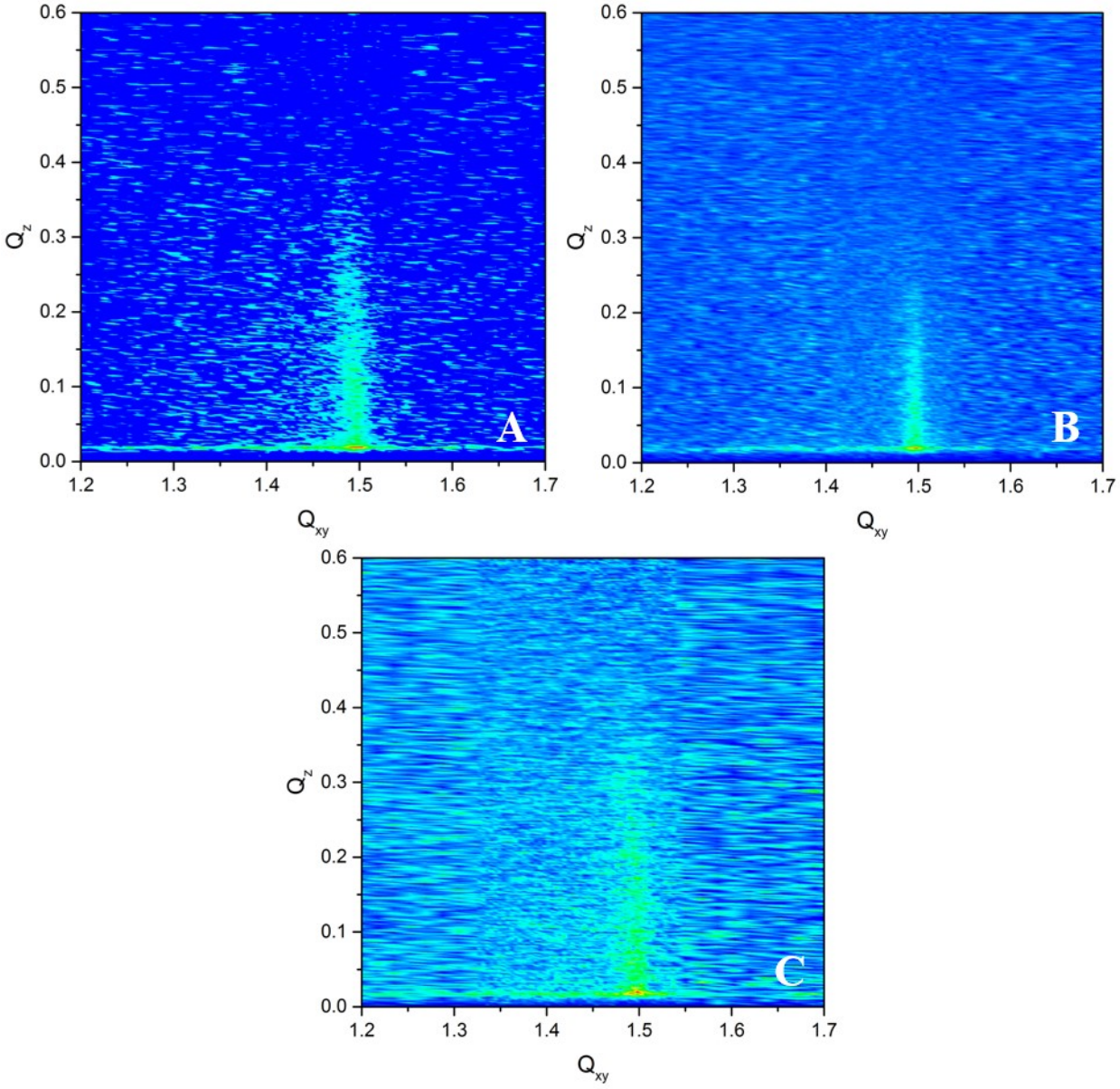

GIXD intensity as a function of the in-plane (Q_{xy}) and out-of-plane (Q_z) components of the scattering vector for an Infasurf monolayer at 35 mN/m in water (A) 0.001 wt% cationic nanoparticles (B) and 0.001% anionic nanoparticles (C).